

**Ion microprobe analyses of oxygen three isotope ratios of chondrules from the Sayh al Uhaymir 290 CH chondrite using a multiple-hole disk**

Daisuke Nakashima<sup>1,2,\*</sup>, Takayuki Ushikubo<sup>1</sup>, Rudraswami N. Gowda<sup>1,†</sup>, Noriko T. Kita<sup>1</sup>,  
John W. Valley<sup>1</sup>, and Keisuke Nagao<sup>2</sup>

<sup>1</sup>WiscSIMS, Department of Geoscience, University of Wisconsin-Madison, Madison, WI 53706, USA

<sup>2</sup>Geochemical Research Center, Graduate School of Science, University of Tokyo, Tokyo 113-0033, Japan

<sup>†</sup>Present address: Geological Oceanography Division, National Institute of Oceanography,  
Dona Paula, Goa-403004, India

\*Corresponding author, Tel: +1-608-261-1523, Fax: +1-608-262-0693,

Email: [naka@geology.wisc.edu](mailto:naka@geology.wisc.edu) (D. Nakashima)

## ABSTRACT

The ion microprobe is the only technique capable to determine high precision stable isotope ratios in individual tiny extraterrestrial particles ( $\leq 100 \mu\text{m}$  in diameter), but these small samples present special analytical challenges. We produced a new sample holder disk with multiple holes (3 holes and 7 holes), in which epoxy disks containing a single unknown sample and a standard grain are cast and polished. Performance tests for oxygen two isotope analyses using olivine standard grains show that the new multiple-hole disks allow accurate analysis of tiny particles if the particles are located within the 500  $\mu\text{m}$  and 1 mm-radius of the center of holes for 7-hole and 3-hole disks, respectively.

Using the new seven-hole disk, oxygen three isotope ratios of eight magnesian cryptocrystalline ( $\sim 100 \mu\text{m}$  in diameter) from the Sayh al Uhaymir (SaU) 290 CH chondrite were analyzed by an ion microprobe at University of Wisconsin. Five out of eight chondrules have nearly identical oxygen isotope ratios ( $\Delta^{17}\text{O} = -2.2 \pm 0.6 \text{‰}$ ; 2SD), which is consistent with those of magnesian cryptocrystalline chondrules in CH/CB and CB chondrites, suggesting a genetic relationship, i.e., formation by a common impact heating event. The other three chondrules have distinct oxygen isotope ratios ( $\Delta^{17}\text{O}$  values from -6.4 ‰ to +2.2 ‰). Given that similar variation in  $\Delta^{17}\text{O}$  values were observed in type I porphyritic chondrules in a CH/CB chondrite, the three chondrules possibly have formed in the solar nebula, similar to the type I porphyritic chondrules.

## INTRODUCTION

Studying tiny extraterrestrial particles ( $\leq 100 \mu\text{m}$  in diameter), such as Antarctic micrometeorites (AMMs), interplanetary dust particles (IDPs), and cometary particles from the Stardust sample return mission, provide important information about the early evolution of the solar system. Stable isotope anomalies of hydrogen, carbon, nitrogen, and oxygen in these tiny particles detected by ion microprobe (or Secondary Ion Mass Spectrometer, SIMS), which are related to stellar nucleosynthesis and to chemical reactions in molecular clouds (Messenger et al. 2003, 2005; Floss et al. 2006; McKeegan et al. 2006; Yada et al. 2008), provide a clue to the prehistory of the solar system. Some particles from comet 81P/Wild 2 (Stardust particles) are similar to Ca-Al-rich inclusions (CAIs) and chondrules in primitive meteorites in terms of mineralogy, chemistry, and oxygen isotope ratios (Zolensky et al. 2006; McKeegan et al. 2006; Nakamura et al. 2008a), suggesting radial transport of high temperature solids formed in the inner solar nebula to the outer solar nebula region. Thus, stable isotope ratios of tiny extraterrestrial particles serve as a useful tracer for the early solar system evolution.

For effective stable isotope analyses of tiny particles using ion microprobes, multiple samples are placed in a single mount (typically 25 mm diameter) and a maximum polished surface area of individual samples is required. In the case of ion microprobe U-Pb zircon geochronology mounts, more than 100 grains of zircon crystals (typically  $\sim 100 \mu\text{m}$  in diameter) are mounted together in a single 25 mm epoxy disk, ground to their mid-sections, and polished. However, for Stardust particles that are precious and with smaller sizes (typically less than  $10 \mu\text{m}$  in diameter), it is difficult to obtain maximum polished surface areas for every particle by a single polishing process. It is important to polish the tiny samples embedded with resins individually to obtain maximum polished surface area. Nakamura et al. (2008a) used a custom-made disk with seven holes, in which multiple individually polished epoxy disks are inserted, and performed oxygen three isotope analyses of Stardust particles using an IMS-1280 at University of Wisconsin (WiscSIMS laboratory). For those analyses, a  $2 \mu\text{m}$  diameter  $\text{Cs}^+$  primary beam was used with typical analytical uncertainties of 1 - 2 ‰ (2SD) for  $\delta^{17}\text{O}$  and  $\delta^{18}\text{O}$  (permil deviations of  $^{18}\text{O}/^{16}\text{O}$  and  $^{17}\text{O}/^{16}\text{O}$  from VSMOW [Vienna Standard Mean Ocean Water]). The 7-hole disk used by

Nakamura et al. (2008a) showed irregular dents around the points that spot-welded a tungsten surface plate and stainless steel disk (the dimension will be described in the next section). The dents may deform electrostatic field on the sample surface. Deformation of electrostatic field modifies the trajectory of secondary ions, which results in isotope fractionation (Kita et al. 2009). In order to avoid any potential problem from the irregular surface and aiming at higher precision and accuracy for analyses, we produced seven-hole disks similar to that used in Nakamura et al. (2008a) (Fig. 1a) and new three-hole disks as modification (Fig. 1b). We performed several tests of oxygen isotope analysis with the multiple-hole disks, and assessed the conditions of highly precise and accurate oxygen isotope analysis for tiny particles. Subsequently, oxygen three isotope ratios of tiny chondrules ( $\sim 100 \mu\text{m}$  in diameter) from the Sayh al Uhaymir (SaU) 290 carbonaceous high-metal (CH) chondrite (Park et al. 2005) were analyzed using the 7-hole disk as an example of the use for unknown samples. The tiny chondrules were extracted previously from the bulk meteorite sample. A fraction of the extracted chondrules were analyzed for noble gases (Nakashima and Nagao 2008). The tiny chondrules are suitable for confirmation of measurement techniques including sample preparation, because they have a similar size to those of AMMs, IDPs and Stardust particles. Furthermore, as described in the next subsection, these chondrules may be related to cryptocrystalline (CC) chondrules in carbonaceous Bencubbin-like (CB) chondrites, which show nearly identical oxygen isotope ratios of  $\Delta^{17}\text{O} = -2.3 \pm 0.6 \text{‰}$  (2SD) (Krot et al. 2010) ( $\Delta^{17}\text{O} = \delta^{17}\text{O} - 0.52 \times \delta^{18}\text{O}$ ). In this respect, we might have selected chondrules with indistinguishable oxygen isotope ratios, which would be useful to evaluate the reproducibility of our analytical protocols on the actual samples.

### **Chondrules in CH Chondrites**

CH chondrites ( $\sim 20 \text{ vol\%}$  of FeNi metal) share petrologic and isotopic characteristics with more metal-rich CB chondrites ( $\sim 70 \text{ vol\%}$  FeNi; Weisberg et al. 1995; Krot et al. 2002). In conjunction with the discovery of the Isheyevo CH/CB chondrite which contains two lithologies: metal-rich CB-like and metal-poor CH-like lithologies (Ivanova et al. 2008), a genetic link between CH and CB chondrites has been suggested (Weisberg et al. 1995; Krot et al. 2002; Ivanova et al. 2008). Furthermore, it was

suggested that the CH and CB metal-rich carbonaceous chondrites are related to cometary materials based on the chemical affinities to Stardust particles (Weisberg and Connolly 2008).

Chondrules in CH chondrites are small ( $\sim 20 - 90 \mu\text{m}$  in diameter on average) relative to those in other chondrites (0.2 - 5 mm), and 79 % of chondrules in CH chondrites are CC type (including radial pyroxene and glassy chondrules) (Scott and Krot 2003). Such non-porphyrritic chondrules formed via complete melting, and their chemistry is considered to have been strongly affected by ambient gas compared to porphyritic chondrules, which formed via incomplete melting. It is expected that the oxygen isotope ratios of CC chondrules can serve as a tracer for the environment of chondrule formation.

CC chondrules in CH and CB chondrites are consistently depleted in volatile lithophile elements including Na and K (Krot et al. 2000, 2001), suggesting that the CC chondrules were isolated from the formation location at elevated temperatures and then cooled rapidly (Krot et al. 2001; Hezel et al. 2003). The abundances of refractory elements such as Ca, Al, and Ti in the CC chondrules are also depleted in variable degrees (Krot et al. 2000, 2001), which is explained by fractional condensation, i.e., more refractory elements condense earlier in the cooling environment (Krot et al. 2001; Hezel et al. 2003; see also Tachibana et al. 2003). In addition, it was reported that magnesian CC chondrules in CH/CB and CB chondrites have similar elemental compositions and show nearly identical oxygen isotope ratios (Krot et al. 2010). Krot et al. (2010) suggested a genetic relationship between the magnesian CC chondrules in the CH/CB and in CB chondrites, i.e., formation by a common heating event induced by large-scale planetesimal impact. Given the chemical affinity between magnesian CC chondrules in CH and CB chondrites (Krot et al. 2000, 2001), one can expect that magnesian CC chondrules in CH chondrites also have similar oxygen isotope ratios to those in magnesian CC chondrules in CH/CB and CB chondrites. Through the mineralogical, chemical, and oxygen isotopic studies of the non-porphyrritic chondrules from SaU 290, we discuss the relationship between magnesian CC chondrules in CH and CB chondrites, which facilitates elucidation of the formation environment of chondrules in metal-rich carbonaceous chondrites.

## FABRICATION OF MULTIPLE-HOLE DISKS

### Seven-hole disks

At the time when Nakamura et al. (2008a) analyzed oxygen three isotope ratios of Stardust particles, the WiscSIMS IMS-1280 could load only two sample holders in vacuum at once (one in the analysis chamber, another in the airlock chamber). For the special requirements of this study, it takes more than a day to reduce the ambient pressure of the analysis chamber containing an epoxy mount in order to reduce  $^{16}\text{OH}^-$  contribution to  $^{17}\text{O}$  signals, especially at low primary ion intensities, even using a liquid  $\text{N}_2$  trap in the analysis chamber. A multiple-hole disk enables a number of samples to be out-gassed without exchanging the sample holder. This is the reason why Nakamura et al. (2008a) employed a 7-hole disk for mounting Stardust particles.

The previous 7-hole disk sample holder (25 mm in diameter), which was used by Nakamura et al. (2008a), consists of two parts (Fig. 1c): an upper disk (3.0 mm thick; stainless steel) with a tungsten plate (100  $\mu\text{m}$  thickness) and a bottom disk (2.0 mm thick; stainless steel). The tungsten plate has seven windows, each with a diameter of 4.0 mm, and is spot-welded on the upper disk that has seven holes each with a diameter of 6.0 mm. The tungsten plate works as a lip to keep the polished sample surface parallel to the disk surface and to make electrical conductivity of the sample surface. Small epoxy disks ( $\sim 5.6$  mm in diameter and  $\leq 1.7$  mm thickness) that contain samples and running standards are put in the upper disk. The bottom disk presses sample surface against the tungsten plate via a spring between sample and the disk, and the bottom disk is screwed to the upper disk (Fig. 1c).

The 7-hole disk used by Nakamura et al. (2008a) showed irregular dents around the welded points on the tungsten plate. In order to avoid any potential problem from the irregular surface (see Introduction), the two new 7-hole disks (disk-1 and disk-2) were fabricated without a welded tungsten-plate (Fig. 1a; disk-1). The new disks have the same dimensions as that of the tungsten-lipped disk, though the upper disks have multiple 4.0 mm diameter windows with a lip machined from a single block of stainless steel. If the surfaces of epoxy disks under the windows are tilted, the measured isotope ratios could be biased (Kita et al. 2009). The flatness of the upper disk surface and epoxy disks was checked

by a ZYGO NewView white light profilometer at the Material Science Center, University of Wisconsin-Madison. The flatness of the entire disk is better than 5  $\mu\text{m}$  and the tilt of individual epoxy disk is less than  $\sim 10 \mu\text{m}$  across the 4.0 mm window. During the fabrication of the disk-1, the internal edges of the lips were made tapered ( $\sim 70 \mu\text{m} / 1.0 \text{mm}$ ) and slope down to the holes, which is expected to reduce deformation of electrostatic field around the lip. The surface of the lip of the disk-2 was flat and consistently 100  $\mu\text{m}$  thick.

### **Three-hole disks**

For Stardust particle studies, epoxy (or acrylic) cylinders with a diameter of  $\sim 8 \text{mm}$  are frequently used (personal communication by M. E. Zolensky). Therefore, multiple-hole disks for the 8 mm epoxy disks were needed. Larger diameter holes reduce total numbers of particles that can be placed in a single holder and require frequent holder exchanges, which may have a disadvantage for achieving ultra-high vacuum ( $<10^{-9}$  torr) during the analyses. However, in 2009, we installed a new storage chamber to the IMS-1280 that can hold up to 6 sample holders. Therefore, it is not so critical to maximize a number of sample disks to be placed in a single sample holder for achieving desirable high vacuum for the oxygen three isotope analyses.

We produced two 3-hole disks (disk-3 and disk-4) with a diameter of 25 mm (Fig. 1b; disk-3). General design of the 3-hole disks is similar to new 7-hole disks, consisting of upper and bottom disks, both of which are machined from single stainless-steel blocks. Compared to the 7-hole disks, a thickness of the upper disk is increased to 4.0 mm so that epoxy disks with maximum thickness of 2.5 mm can be mounted. The three holes in the upper disks have a diameter of 8.0 mm with a 6.0 mm diameter window and a 100  $\mu\text{m}$  lip. The centers of the three holes are located at 5 mm from the center of the whole disk, which is 5 mm away from the outer lip of the CAMECA holder (Fig. 1b) that has another 100  $\mu\text{m}$  thickness. In the case of the 7-hole disks, the centers of outer six holes are located 7.5 mm from the center of the whole disk, which is much closer to the edge of the outer lip (2.5 mm). Wide windows and proximity of hole centers to the disk center are expected to reduce deformation of the surface electrostatic field. Thickness of the bottom disks and mounting procedure of epoxy disks are the same as

those for 7-hole disks (Fig. 1c).

## **SAMPLE PREPARATION**

### **Standard olivine grains for test analyses**

Epoxy disk preparation procedures are similar to those of Nakamura et al. (2008a). A rod made of epoxy resin (5.6 mm or 7.8 mm in diameter and ~ 10 - 15 mm in length) that has a mesa with a  $1 \times 1$  mm square top is prepared (Fig. 1d). A particle to be analyzed and a running standard are placed on the top, and fixed with a drop of epoxy resin. The mesa is then covered with a plastic tube and filled with epoxy. The epoxy rod is ground and polished using diamond lapping film until the maximum surface area of the particle is exposed. Thus, the particle and running standard are precisely located within the  $1 \times 1$  mm square on the center of the epoxy disk, which is important for isotope analyses using multiple-hole disks. Finally, the bottom of the rod is cut off at ~ 1.5 - 1.7 mm for 5.6 mm epoxy disks (or 2.0 - 2.5 mm for 7.8 mm epoxy disk) from the polished surface.

### **Chondrule samples**

More than three hundred tiny spherical chondrules (100 - 200  $\mu\text{m}$  in diameter; Fig. 2) were previously extracted from the bulk sample of SaU 290 (~ 1.5 g) by a freeze-thaw cycling (~ 50 times) and crushing in a cylinder mortar for noble gas analyses of individual chondrule (Nakashima and Nagao 2008). Eight chondrules (Ch01 - Ch09; Ch03 is unused) were selected randomly for this study from the extracted chondrules.

We followed sample preparation and observation processes of Nakamura et al. (2008a). After the chondrules were examined by synchrotron radiation X-ray diffraction (SR-XRD), all eight chondrules were individually embedded in epoxy disks with San Carlos olivine (SC-Ol) running standard grains for oxygen isotope analysis, and the maximum polished surface area was obtained for chondrules. In two epoxy disks, the SC-Ol grains were not exposed on the surface (Ch04 and 09). The SC-Ol grain in the center hole mounted in the 7-hole disk was used as the running standard for these two chondrule analyses.



## **ANALYTICAL METHOD**

### **Synchrotron Radiation X-Ray Diffraction**

Bulk mineralogy of five chondrules was investigated by SR-XRD at the Institute of Material Structure Science, High Energy Accelerator Organization (Tsukuba, Japan). The chondrules were mounted on a thin glass fiber (5  $\mu\text{m}$  in diameter) and exposed to monochromatic X-rays ( $\lambda = 2.166$  and  $2.164$   $\text{\AA}$ ; two sessions). Clear X-ray powder photographs were taken using a Gandolfi camera with an exposure to synchrotron X-rays of less than 30 min (Nakamura et al. 2008b).

### **Electron Microscopy**

The backscattered electron (BSE) images of the polished surface of chondrules were obtained using a scanning electron microscope (SEM; Hitachi S3400) with an energy-dispersive X-ray spectrometer (EDS) at University of Wisconsin-Madison. Elemental compositions of the chondrules were measured with an electron probe microanalyzer (EPMA; CAMECA SX-51) equipped with five wavelength-dispersive X-ray spectrometers (WDSs) at University of Wisconsin-Madison. WDS quantitative chemical analyses of individual silicate phases were performed at 15 kV accelerating voltage and 6 - 20 nA beam current with a focused beam of  $\sim 1$   $\mu\text{m}$  in diameter. Analyses of bulk chondrule chemical compositions were performed using 15 kV accelerating voltage and 10 nA beam current with a defocused beam of  $\sim 25$   $\mu\text{m}$  in diameter.

### **Oxygen isotope Analyses**

We applied three different conditions for oxygen isotope analyses with the CAMECA IMS-1280 ion microprobe at the WiscSIMS Lab: 1) the routine oxygen two isotope analysis ( $^{18}\text{O}/^{16}\text{O}$ ) using 10  $\mu\text{m}$  spots (Kita et al. 2009) for multiple-hole disk tests, 2) oxygen three isotope analysis with 15  $\mu\text{m}$  spots (Kita et al. 2010) for chondrules from SaU 290, and 3) oxygen three isotope analysis with  $\sim 4$   $\mu\text{m}$  spots for selected chondrule samples. The condition 3) is similar to that in Nakamura et al. (2008a) for Stardust sample analyses, though we used slightly larger beam size and reduced the analysis time per single spot. After SIMS analysis, all SIMS pits were observed with the SEM at University of Wisconsin-Madison to confirm the analyzed positions.

### *Conditions of analyses*

For the test analyses of the multiple-hole disks, a focused  $\text{Cs}^+$  primary beam was set to a size of  $\sim 10 \mu\text{m}$  diameter at the intensity of  $\sim 2.0 \text{ nA}$ , and was accelerated by a 20 kV total potential (10 kV in a primary column and -10 kV on the sample). A normal incidence electron gun was used for charge neutralization. Secondary ions of  $^{16}\text{O}^-$  and  $^{18}\text{O}^-$  were accelerated at -10 kV to the detectors with high secondary ion transmission. Secondary ion optics was configured similarly to those by Kita et al. (2009): transfer lens magnification of  $\times 200$ , contrast aperture  $400 \mu\text{m}$  in diameter, field aperture  $4000 \times 4000 \mu\text{m}$ , entrance slit width  $120 \mu\text{m}$ , energy slit width 40 eV, and exit slit width  $500 \mu\text{m}$  (mass resolving power  $\sim 2000$ ). Multi-collection Faraday Cups (FCs) were used to measure  $^{16}\text{O}^-$  and  $^{18}\text{O}^-$  simultaneously. Typical count rate of  $^{16}\text{O}^-$  was  $3 \times 10^9$  cps (converted from ion current). The baseline of the FC amplifiers was measured once before starting the analysis session.

For the oxygen three isotope analyses of the SaU 290 chondrules, two sizes of focused  $\text{Cs}^+$  primary beams ( $10 \times 15 \mu\text{m}$  at the intensity of  $\sim 2.5 \text{ nA}$  and  $3 \times 4 \mu\text{m}$  at  $\sim 28 \text{ pA}$ ) were applied. Other conditions are generally similar to oxygen two isotope analyses, otherwise described below. The entrance slit width was set to  $75 \mu\text{m}$ . The secondary  $^{17}\text{O}^-$  ions were detected by using mono-collector at the ion optical axis and fixed position. The exit slit width for mono-collector detecting  $^{17}\text{O}^-$  ions was set to  $240 \mu\text{m}$  (mass resolving power  $\sim 5000$ ) and  $200 \mu\text{m}$  (mass resolving power  $\sim 6000$ ) in the sessions with  $15 \mu\text{m}$  spots and with  $4 \mu\text{m}$  spots, respectively, which were sufficient to clearly separate  $^{17}\text{O}$  and  $^{16}\text{O}^1\text{H}$  peaks. For detection of minor isotopes  $^{17}\text{O}^-$  and  $^{18}\text{O}^-$ , FC detectors were used in the session with  $15 \mu\text{m}$  spots and electron multipliers (EM) in the session with  $4 \mu\text{m}$  spots. In the session with  $4 \mu\text{m}$  spots, the field aperture was set to  $3000 \times 3000 \mu\text{m}$ . In these conditions, intensities of  $^{16}\text{O}$  were  $2.6 \times 10^9$  and  $1.6 \times 10^7$  cps with  $15 \mu\text{m}$  and  $4 \mu\text{m}$  primary beams, respectively. The baselines of FCs were measured during the presputtering (100 sec for  $15 \mu\text{m}$  spots and 360 sec for  $4 \mu\text{m}$  spots) in respective analyses, and used for data correction. The contribution of  $^{16}\text{O}^1\text{H}^-$  tail interference to the  $^{17}\text{O}^-$  signal was corrected by the method described in Heck et al. (2010), though the contribution was negligibly small ( $\leq 0.1 \text{ ‰}$ ).

### *Instrumental bias corrections and precision of analyses*

For correction of instrumental mass fractionation (instrumental bias), San Carlos olivine (SC-Ol;  $\delta^{18}\text{O} = 5.32 \text{ ‰}$  VSMOW, Kita et al. 2010), three kinds of low-Ca pyroxene (En97, En90, and En85), and diopside were used for the session with 15  $\mu\text{m}$  spots, while for the session with 4  $\mu\text{m}$  spots SC-Ol, low-Ca pyroxene with En97, and diopside were used.

Actual chondrules also contain minor olivine, glass and silica phases, which overlap within a beam of 15  $\mu\text{m}$  spot analyses. We corrected instrumental bias assuming as low-Ca pyroxene, except for a silica-bearing chondrule, because these minor phases have small volume and instrumental bias similar to that of low-Ca pyroxene (within a few ‰, Valley and Kita 2009). In the 4  $\mu\text{m}$  spot analyses of pyroxene, instrumental biases were corrected for individual pyroxene using their respective Wo contents (by linear interpolation between enstatite and diopside standards, Kita et al. 2010). For a chondrule containing silica (for both 15  $\mu\text{m}$  and 4  $\mu\text{m}$  spot analyses), instrumental bias was corrected as a mixture of low-Ca pyroxene and silica by estimating their relative fractions from the bulk chemical composition of the chondrule. The instrumental bias correction factor of -9 ‰ relative to SC-Ol is assumed (Valley and Kita 2009). These instrumental bias corrections are mass-dependent, thus do not affect  $\Delta^{17}\text{O}$  values.

In the session with 15  $\mu\text{m}$  spots, three spots were analyzed in individual chondrules, bracketed by six to eight sets of analyses on the SC-Ol grains mounted with the chondrules, while five to eight spots were analyzed in the chondrules in the session with 4  $\mu\text{m}$  spots, bracketed by six sets of analyses on the SC-Ol grains. In the two samples where the SC-Ol grain was not exposed on the polished epoxy surface, the SC-Ol grain in the center hole was used as the running standard for the chondrule analyses. External reproducibility of 15  $\mu\text{m}$  spot analyses of the SC-Ol grains was 0.2 - 1.8 ‰ for  $\delta^{18}\text{O}$ , 0.5 - 1.6 ‰ for  $\delta^{17}\text{O}$ , and 0.5 - 0.9 ‰ for  $\Delta^{17}\text{O}$  (2SD), while that of 4  $\mu\text{m}$  spot analyses was 0.7 - 1.8 ‰ for  $\delta^{18}\text{O}$ , 0.7 - 1.6 ‰ for  $\delta^{17}\text{O}$ , and 0.7 - 1.1 ‰ for  $\Delta^{17}\text{O}$  (2SD). In one sample, SC-Ol standard mounted in the epoxy disk was relatively smaller ( $\sim 70 \mu\text{m}$ ) than other mounts and the external reproducibility was poor (1.8 ‰ and 1.6 ‰ for  $\delta^{18}\text{O}$  and  $\delta^{17}\text{O}$ , 2SD, respectively), though it did not affect the reproducibility of  $\Delta^{17}\text{O}$  data significantly.

## PERFORMANCE TEST OF MULTIPLE-HOLE DISKS

As test analyses of the multiple-hole disks, we measured oxygen two isotope ratios of SC-OI standard grains mounted in epoxy disks at WiscSIMS. The reproducibility of oxygen isotope ratios among different holes and within the individual holes in the multiple-hole disks were used to evaluate the performance of the disks.

### **Test-1: Inter-hole instrumental mass biases relative to the center hole**

For the test session of the 7-hole disk-1, four epoxy disks which contain SC-OI grains (~ 0.1 - 1 mm in diameter) were loaded in the center, west, northwest, and northeast holes (Fig. 1a), and rest of the holes were filled by quartz glass disks with a diameter of 5.6 mm. Three sets of analyses were made on the center of the SC-OI grains in the outer holes, bracketed by eight sets of analyses ( $\pm 0.3$  ‰, 2SD) at the center of the SC-OI grain in the center hole before and after. Next, disk-1 was rotated 180 degrees within the CAMECA holder so that east, southeast, and southwest holes were analyzed. Like the first sub-session, three sets of analyses in the outer holes were made, bracketed by eight sets of analyses in the center hole. Variation of  $\delta^{18}\text{O}$  in SC-OI grains in outer holes relative to the SC-OI grain in the center hole is within  $\pm 1$  ‰ (Fig. 3a; see also Table 1), which is comparable to the results of test analyses using the tungsten-lipped disk (Nakamura et al. 2008a). Secondary ion yields ( $^{16}\text{O}$  count rate / primary beam current; units are  $10^9$  cps/nA) were comparable [94 - 102 %;  $(1.27 - 1.38) \times 10^9$  cps/nA] to those at the center ( $1.35 \times 10^9$  cps/nA on average).

For the test session of the 7-hole disk-2, seven epoxy disks containing SC-OI grains (0.5 - 2 mm in diameter) were loaded, filling all the holes. Four sets of analyses were made on the center of the grains in the outer holes, bracketed by eight sets of analyses ( $\pm 0.22$  ‰, 2SD) at the center of the grain in the center hole before and after. Variation of  $\delta^{18}\text{O}$  in SC-OI grains in outer holes relative to the SC-OI grain in the center hole is within  $\pm 0.5$  ‰ (Fig. 3b; see also Table 1), which is better than the disk-1. Secondary ion yields were comparable (92 - 101 %) to those at the center. Since deformation of electrostatic field should reflect the geometries around the respective holes including the outer lip of the

CAMECA holder, isotopic fractionation is expected to be related to the hole position within the disks (X-Y effect; cf., Kita et al. 2009). However, comparing the test results of disk-1 and -2 (Fig. 3), the  $\delta^{18}\text{O}$  variation does not appear to be related to hole positions, i.e., no detectable geometric effect on  $\delta^{18}\text{O}$  in the 7-hole disks overall.

For the test session of the 3-hole disks (disk-3 and disk-4), six epoxy disks ( $\sim 7.8$  mm diameter) containing SC-OI grains (1 - 4 mm in diameter) were loaded in all of the holes. Four sets of analyses of  $\delta^{18}\text{O}$  were made on the center of the grains in the southeast and southwest holes, bracketed by eight sets of analyses ( $\pm 0.14$  ‰ for disk-3 and  $\pm 0.21$  ‰ for disk-4, 2SD) at the center of the grain in the north hole before and after. The  $\delta^{18}\text{O}$  variation of SC-OI grains in southeast and southwest holes relative to the SC-OI grain in the north hole is within  $\pm 0.5 - 0.7$  ‰ (Fig. 4; see also Table 2). Secondary ion yields were comparable (93 - 100 %) to those at the center. Like the 7-hole disks, no geometric effect on  $\delta^{18}\text{O}$  in the disks overall was observed.

### **Test-2: Intra-hole instrumental mass biases**

We observed  $\delta^{18}\text{O}$  variation at different locations (north, south, east, and west) in each hole. In the two large SC-OI grains ( $\sim 0.5 \times 1$  mm; center and west; first sub-session) in the disk-1,  $\delta^{18}\text{O}$  variations at different locations relative to the center of the grains were  $\pm 0.5$  ‰ (Online supplements). Secondary ion yields were 97 - 103 % relative to those of center of the grains. In disk-2 (all the holes),  $\delta^{18}\text{O}$  variations were  $\pm 0.5$  ‰ within a  $\sim 500$   $\mu\text{m}$ -radius from the center of respective holes (Online supplements). Secondary ion yields were 92 - 104 % relative to those of center of the grains. If analyzing further from the center of the mount (up to 1 mm-radius), relative  $\delta^{18}\text{O}$  values sometimes exceeded the  $\pm 1$  ‰ range, and secondary ion yields decreased to 79 %. These results show that oxygen isotope analyses performed within a  $\sim 500$   $\mu\text{m}$ -radius of the center of each hole do not have significant analytical bias. Using flat quartz glass disks, it was found that the secondary ion yields decrease by  $\sim 5$  % outside of 1 mm-radius. This indicates that the electrostatic field may be more deformed towards the lip of the window, which may lead to deviations of the secondary ion trajectory even though automatic centering of the secondary ions to the field aperture is applied (Kita et al. 2009).

For the 3-hole disks,  $\delta^{18}\text{O}$  variations at different locations (north, south, east, and west) in respective holes were within  $\pm 0.5$  ‰ when measuring within a  $\sim 1$  mm-radius from the center of respective holes, and secondary ion yields were 91 - 102 % relative to those of center of the grains (Online supplements). Outside of the 1 mm-radius, relative  $\delta^{18}\text{O}$  values exceeded the 1 ‰ range, though relative secondary ion yields were 91 - 98 %. Thus, oxygen isotope analyses performed within the 1 mm-radius of the center of each hole may not show significant analytical bias due to location of sample.

### **Evaluation of multiple-hole disks**

The test analyses show that the new multiple-hole disks are applicable to tiny particle analysis of  $\delta^{18}\text{O}$  with precision of  $\pm 0.5$  ‰ (2SD) as long as the particles are located within the radius of  $\sim 500$   $\mu\text{m}$  and 1 mm of the center of holes for 7-hole disks and 3-hole disks, respectively. The requirement for particle location is met by the sample preparation procedures described above (see Sample preparation). It is important to mount running standards with samples in the same epoxy disks so as to correct unexpected instrumental fractionation (see the next section). The level of reproducibility at 0.5 ‰ is somewhat worse than that typically obtained from flat 25 mm mounts without significant topography ( $\pm 0.3$  ‰; Kita et al. 2009). Therefore, the use of multiple-hole sample mounts creates a trade-off of precision and accuracy vs. analysis of a single flat 25 mm mount. However, the analytical uncertainty of  $\delta^{18}\text{O} \pm 0.5$  ‰ is still smaller than that for analyses with small spots in this study and for Stardust particles (Nakamura et al. 2008a) at the level of 0.7 - 2 ‰, and does not become a problem for the small spot analyses.

For data obtained from outside of 0.5 ‰ area, we observed systematic change in  $\delta^{18}\text{O}$  values that depended on the location of analyses relative to the center of each hole (Fig. 5). As shown in Fig. 5a (7-hole disks), the relative  $\delta^{18}\text{O}$  values are high in north and east positions, while they are low in the south and west. The 3-hole disks show distribution of relative  $\delta^{18}\text{O}$  values similar to that for the 7-hole disks (Fig. 5b), though  $\delta^{18}\text{O}$  variation is less pronounced for the 3-hole disks. Thus, unlike comparison of relative  $\delta^{18}\text{O}$  values among holes, there is a relationship between relative  $\delta^{18}\text{O}$  values at different locations in each hole and directions, which is so called the X-Y effect (Kita et al. 2009). However, the

trend we observed is opposite to that in Kita et al. (2009) who measured grains with surface topography due to polishing relief in a single flat 25 mm mount. Slightly convex surfaces of individual grains are common in zircon geochronology and other grain mounts (Kita et al. 2009). This contrasts with the disks with multiple holes, the sample surface is 100  $\mu\text{m}$  deeper than the lip of the disk (i.e., small dimples vs. small bumps). The deformation of the electrostatic field above the sample surface in the multiple-hole disks would thus be in the opposite direction compared to that of zircon grains with polishing relief. Thus, the X-Y effects we observe likely result from the specific geometry of the multiple-hole disks. The 3-hole disks have wider windows and holes closer to the disk center, which reduce deformation of electrostatic field on the sample surface. As a result, the  $\delta^{18}\text{O}$  variations in the 3-hole disks are smaller than that of 7-hole disks.

## **ANALYSES OF THE SAU 290 CHONDRULES**

### **Mineralogy and chemistry of the SaU 290 chondrules**

We studied 8 cryptocrystalline (CC) chondrules. All eight chondrules have spherical shape and their sizes range from 60  $\mu\text{m}$  to 160  $\mu\text{m}$  in diameter. They show various colors under an optical microscope before mounting: white-clouded/transparent and black opaque (Fig. 2; Table 3). We recognized that the chondrules mainly consist of low-Ca pyroxene by SR-XRD (Fig. 8). All crystalline chondrules exhibit fine-grained texture with BSE images (Figs. 6-7), indicating that they are CC chondrules. Three opaque chondrules (Ch01, 02, and 07) contain tiny Fe metal grains ( $< 1 \mu\text{m}$  in diameter; detected by SEM-EDS; Figs. 6-7), while others are free from Fe metal grains. The opacity may be due to the presence of the numerous tiny Fe metal grains (Read 1986). Except for the relationship between tiny Fe metal grains and opacity, there appears to be no relationship between the optical properties and texture (or chemistry) for CC chondrules (discussed in the next section). It is not surprising to find all eight chondrules are CC type despite random selection, because  $\sim 80\%$  of the chondrules in CH chondrites are CC type (Scott and Krot 2003). In addition, the initial selection of  $\sim 300$  chondrules are biased to only spherical chondrules in order to avoid potential matrix materials (Nakashima and Nagao 2008), which biased our selection towards non-porphyritic chondrules and away from porphyritic chondrules having irregular

shapes (e.g., Wasson 1996).

For CC chondrules, the estimated bulk chemical compositions obtained by defocused-EPMA are close to stoichiometric magnesian low-Ca pyroxene with Mg# (molar %  $[\text{MgO}]/[\text{MgO}+\text{FeO}] > 98$  (Fig. 9; Table 3). This is consistent with the fact that magnesian CC chondrules are dominant in CH chondrites (e.g., Scott 1988). The bulk chemical compositions of Ch02, 04, 05, 07, and 08 are deviated slightly from stoichiometric low-Ca pyroxene (Fig. 9). The SR-XRD patterns of Ch02, 04, and 05 (no SR-XRD data for Ch07 and Ch08) show reflection lines of olivine in addition to low-Ca pyroxene (Figs. 8a-c). Although we did not recognize olivine crystals by SEM observation, chemical composition data of these chondrules with focused-EPMA appear to be mixture of low-Ca pyroxene and olivine (~ 15 % contribution of olivine), suggesting olivine and low-Ca pyroxene occur as smaller grains than elastic scattering volume of electrons (a few  $\mu\text{m}$  in diameter) by EPMA. The slightly high (Mg+Fe)/Si ratios (Fig. 9) are consistent with a small contribution of olivine (11 - 16 %). In Ch02, we identified two phases (Figs. 6b and 7b). The brighter phase has higher Si/Mg atomic ratios (~ 0.87) and  $\text{Cr}_2\text{O}_3$  content (0.71 wt%) than darker phase (Si/Mg atomic ratios of 0.80 - 0.84, and  $\text{Cr}_2\text{O}_3$  content of 0.39 wt%; Table 4). In the enlarged BSE image (Fig. 7b), the darker phase shows dendritic texture, suggestive of supercooling (Lofgren 1996). As in the case of Ch02, with a high magnification and enhanced contrast BSE images, we found fine textures in individual CC chondrules (Fig. 7) that can explain the observed variation of the bulk chemical compositions. The bulk chemical composition of Ch01 is slightly shifted towards anorthite from stoichiometric low-Ca pyroxene (Fig. 9), indicating a small contribution of anorthite component (13 % on average). Low-Ca pyroxene occurs as fan-like laths (~ 1  $\mu\text{m}$  in width; ~ En96Wo3; Lpx in Figs. 6a and 7a) with feldspathic glass (~ An56Ab34; Table 4). Note that accuracy of chemical compositions of low-Ca pyroxene and glass by focused-EPMA is limited because of the small grain size of the two phases. In glass, secondary alteration phases such as nepheline or sodalite were not observed, suggesting that Ch01 escaped secondary alteration. High-Ca pyroxene (Hpx, 5 - 15  $\mu\text{m}$  in diameter; En77Wo22; Table 4) occurs with tiny Fe-metal grains (< 1  $\mu\text{m}$  in diameter) on the periphery of Ch01 (Figs. 6a and 7a). The bulk chemical composition of Ch06 is slightly enriched in Si relative to



others. Ch06 shows fine-grained texture (Figs. 6e and 7d), and consists mainly of two types of low-Ca pyroxene (En94Wo5 with 1 - 5  $\mu\text{m}$  in diameter and En98Wo1 with 7 - 10  $\mu\text{m}$  in diameter), and SiO<sub>2</sub>-rich phase (1 - 2  $\mu\text{m}$  in diameter; SiO<sub>2</sub> ~ 80 wt%) as shown in Table 4. It is concluded from the SR-XRD pattern that SiO<sub>2</sub>-rich phase is cristobalite (Fig. 8d). Focused-EPMA that aimed SiO<sub>2</sub>-rich phase detected certain amounts of Al<sub>2</sub>O<sub>3</sub>, MgO and CaO (Table 4), which may be contaminant from surrounding pyroxene because the size of SiO<sub>2</sub>-rich phase is comparable (or smaller) to the scattering volume of electrons by focused-EPMA (a few  $\mu\text{m}$  in diameter). Thus, Ch06 is a silica-bearing chondrule. A contribution of silica to the whole chemical compositions is 14 % on average.

The bulk chemical composition of Ch09 was not obtained with defocused-EPMA due to many voids (Fig. 6h), which results in low oxide total and, unreliable data. Focused-beam EPMA data (avoiding voids) showed chemical composition of Ch09 is close to low-Ca pyroxene (En94Wo5; not shown in Fig. 9; analytical totals ~ 80 - 97 wt%), which is consistent with the SR-XRD pattern for this chondrule that only shows reflection lines of low-Ca pyroxene (Fig. 8e). Thus, Ch09 is also a magnesian pyroxene-dominated CC chondrule.

The CI-normalized elemental abundances of CC chondrules (Fig. 10; Ch09 are not plotted) are within the range of chondrules in other CH chondrites (Krot et al. 2000). The five “typical” CC chondrules (Ch02, 04, 05, 07, and 08) are depleted in refractory and volatile elements, like CC chondrules in other CH chondrites (Fig. 10; Krot et al. 2000). Compared to other typical CC chondrules, Ch01 and 06 are enriched in refractory elements and volatile elements, respectively (Fig. 10). The refractory element abundances in Ch01 exceed those of CI chondrites by the factor of 2, which makes Ch01 to be relatively “refractory-rich” chondrule. Thus, eight chondrules in this study include typical, refractory-rich, silica-bearing CC chondrules.

### **Oxygen isotope ratios**

In the first session (session 1), chondrules were analyzed with 15  $\mu\text{m}$  spots, except for Ch09 that has a porous texture at a scale much smaller than the SIMS beam spots. In the second session (session 2), selected chondrules (Ch01, 02, 04, 06, and 09) were analyzed with 4  $\mu\text{m}$  spots to examine internal

isotope heterogeneity.

At the time of the session 1, chondrules Ch02, 05, 06, 07, and 08 were first loaded to disk-1 at the outer holes for the SIMS analyses, because we only had one 7-hole disk fabricated. After these five chondrules were analyzed, the sample holder was removed from the instrument and the rest of the chondrules Ch01 and 04 were loaded to the same disk for the analysis. As described earlier, a standard olivine grain in the epoxy disk of Ch04 was not exposed to the surface, and therefore standard olivine at the center hole was used as a running standard. The raw measured  $\delta^{18}\text{O}$  values of SC-Ol grains in the center hole and in an outer hole with Ch01 agreed within 0.5 ‰ (Fig. 11), as we expect from the performance test (Fig. 3). However, during the analyses of first set of chondrules, it was observed that raw  $\delta^{18}\text{O}$  values of SC-Ol grains in the outer holes are consistently lower by 1 ‰ than that of the center grain (Fig. 11). The cause of lower  $\delta^{18}\text{O}$  values in outer holes were not identified, though it may be related to sample preparation such as position of epoxy disks within the holes and position of the 7-hole disk within the CAMECA holder. For samples in the first disk, standard olivine grain in each of the outer holes was used to correct instrumental bias. The bias between the central hole and outer holes did not affect any actual data after the instrumental bias corrections. However, this situation would cause systematic error if the standard grain had not been mounted with each unknown chondrule sample that was analyzed during the first set of session 1. Thus, it is very important to mount running standards with samples in the same epoxy disks so as to correct (unexpected) instrumental fractionation. It should be mentioned that raw  $\delta^{18}\text{O}$  and  $\delta^{17}\text{O}$  values of standard in the outer disk shift along the slope 0.5 mass fractionation line (Fig. 11). Therefore, results obtained without standard grain in the same epoxy disk have no measurable effect on the  $\Delta^{17}\text{O}$  values.

Oxygen isotope analyses of seven chondrules with 15  $\mu\text{m}$  spots are shown in Fig. 12a. These data plot along a slope-1 line between the Carbonaceous Chondrite Anhydrous Mineral (CCAM) and Young and Russell (Y&R) lines (Fig. 12). Five chondrules (Ch02, 04, 05, 07, and 08) plot within a narrow range of isotope ratios with the average  $\Delta^{17}\text{O}$  value of  $-2.2 \pm 0.6$  ‰ (2SD; Fig. 13). The other two chondrules have distinct  $\Delta^{17}\text{O}$  values;  $-6.4$  ‰ in Ch06 and  $+2.2$  ‰ in Ch01, as shown in Fig. 13. Data

from three 15  $\mu\text{m}$  spots in each chondrule are consistent within the analytical uncertainties (Fig. 12a; Table 5). The constituent mineral phases of the chondrules are much smaller than 15  $\mu\text{m}$ , and therefore the derived oxygen isotope ratios represent average values.

Oxygen isotope analyses of Ch01, 02, 04, and 06 with 4  $\mu\text{m}$  spots are shown in Fig. 12b. In Ch01, 02, and 04, results of 4  $\mu\text{m}$  spot analyses in pyroxene grains with different chemical compositions do not show any resolvable internal isotope heterogeneity beyond analytical uncertainties (Fig. 12b; Table 6). The average  $\delta^{18}\text{O}$ ,  $\delta^{17}\text{O}$ , and  $\Delta^{17}\text{O}$  values of Ch01, 02 and 04 are generally in good agreement with those obtained from 15 $\mu\text{m}$  spot data. However, oxygen isotope ratios analyzed with 4  $\mu\text{m}$  spots (Fig. 12b) are slightly shifted to the right relative to those analyzed with 15  $\mu\text{m}$  spots (Fig. 12a), i.e., the  $\delta^{18}\text{O}$  values are slightly higher (+0.9 ‰ on average; Tables 5 and 6). Difference of  $\sim 1$  ‰ between data in  $\delta^{18}\text{O}$  values of two sessions are only marginal compared to the analytical uncertainties (0.7 - 1.8 ‰) of the second session. The measured  $\delta^{18}\text{O}$  and  $\delta^{17}\text{O}$  values in Ch06 using 4  $\mu\text{m}$  spots show a large variation along the slope of  $\sim 0.5$ , which appears to be correlated with the fraction of silica phase as revealed by the examination of the analyses pits after using SEM. The 4  $\mu\text{m}$  primary beam size was comparable to the grain sizes of pyroxene and silica in the chondrule (Fig. 7d). The volume fractions of silica within the pits were difficult to estimate. Thus, data are corrected using the same instrumental biases as that used for 15  $\mu\text{m}$  spot analyses (e.g., average fractions of pyroxene and silica), which do not accurately correct contribution of silica at each analysis point. Therefore, the variations of Ch06 data in Fig. 12b along slope 0.5 are not true variations, but analytical artifacts.

Chondrule Ch09 was only analyzed in the session with 4  $\mu\text{m}$  spots in order to avoid numerous void spaces within the sample (Fig. 6h). However, SEM observation after the SIMS analyses revealed that all the SIMS pits more or less overlapped the voids. As a result, the  $^{16}\text{O}$  count rates during the analyses were significantly lower ( $\sim 60$  %) than those of other chondrules and SC-OI standard grains, and the internal errors associated with the isotope ratios are about 1.4 times higher than those of the SC-OI standard grain (Online supplements). The measured  $\delta^{18}\text{O}$  and  $\delta^{17}\text{O}$  values from multiple spot analyses in Ch09 scattered significantly more than those in other chondrules, in the range as large as 10 ‰ in  $\delta^{18}\text{O}$ ,

possibly due to the effect of charging by the presence of voids within the analysis areas. However,  $\Delta^{17}\text{O}$  values of multiple analyses were reproducible within analytical uncertainty with the average value of  $-6 \pm 2 \text{ ‰}$  (Online supplements). Thus, in spite of poor analytical conditions, Ch09 seems to be another relatively  $^{16}\text{O}$ -rich chondrule similar to Ch06.

## **FORMATION ENVIRONMENT OF THE SAU 290 CHONDRULES**

The average  $\Delta^{17}\text{O}$  value of  $-2.2 \pm 0.6 \text{ ‰}$  (2SD; Fig. 13) observed in the five chondrules (Ch02, 04, 05, 07, and 08) is consistent with those of magnesian CC chondrules in CH/CB and CB chondrites (Krot et al. 2010) and close to those of the most CC chondrules in other CH chondrites (Yoshitake and Yurimoto 2004; Jones et al. 2005; Yurimoto et al. 2008). In addition, the five chondrules are chemically “typical” in terms of depletion in refractory and volatile elements, like CC chondrules in CH and CB chondrites (Fig. 10; Krot et al. 2000, 2001). The identical oxygen isotope ratios and chemical affinity support the view that most of the magnesian CC chondrules in CH and CB chondrites formed together from an isotopically uniform gaseous reservoir generated by an impact event (Krot et al. 2010).

Three other chondrules have distinct  $\Delta^{17}\text{O}$  values ( $\sim +2.2 \text{ ‰}$  for refractory-rich Ch01,  $\sim -6.4 \text{ ‰}$  for silica-bearing Ch06, and  $\sim -6 \text{ ‰}$  for porous Ch09) that obviously could not be formed by the impact heating event common to other magnesian CC chondrules with  $\Delta^{17}\text{O}$  value of  $-2.2 \text{ ‰}$ . The positive  $\Delta^{17}\text{O}$  values of  $\sim +2.2 \text{ ‰}$  in Ch01 are rare for chondrules in carbonaceous chondrites, because carbonaceous chondrite chondrules generally show negative  $\Delta^{17}\text{O}$  values (cf., Krot et al. 2006). Many ordinary chondrite chondrules and a subset of enstatite chondrite chondrules have positive  $\Delta^{17}\text{O}$  values ( $\leq +1.6 \text{ ‰}$ ; Clayton et al. 1991; Kita et al. 2010; Weisberg et al. 2010), though the  $\Delta^{17}\text{O}$  value of Ch01 is higher than those of chondrules in ordinary and enstatite chondrites and close to those of chondrules in a Rumuruti group (R) chondrite (Greenwood et al. 2000). The chondrules in an R chondrite contain a certain amount of iron (Fa10 and Fs5-7; Greenwood et al. 2000), while Ch01 is almost iron-free (Fs < 1). There appears to be no chemical affinity between Ch01 and the chondrules in an R chondrite.

Among carbonaceous chondrite chondrules, chondrules in metal-rich carbonaceous chondrites exceptionally show positive  $\Delta^{17}\text{O}$  values (Yoshitake and Yurimoto 2004; Yurimoto et al. 2008; Krot et al.

2010). Type I porphyritic chondrules in a CH/CB chondrite have  $\Delta^{17}\text{O}$  values from -5 ‰ to +4 ‰ and were suggested to have been a nebular product but not a product of the impact event that formed magnesian CC chondrules (Krot et al. 2010). The range of  $\Delta^{17}\text{O}$  values of Ch01, 06, and 09 (-6 ‰ to +2.2 ‰) are within (similar to) that of the type I porphyritic chondrules (Krot et al. 2010). It may be possible that these chondrules with distinct  $\Delta^{17}\text{O}$  values formed together with the type I porphyritic chondrules in the solar nebula.

The difference in chemical compositions of Ch01, 06, and 09 (Fig. 10) can be explained by fractional condensation in the solar nebula, i.e., more refractory elements condensed earlier in the cooling environment of solar composition and the condensates were isolated from the reactive environment (see Introduction). If the CC chondrules formed by the formation sequence, refractory-rich Ch01 condensed earlier than Ch06 and 09 (Fig. 10 and Table 3; Ca/Si and Al/Si ratios of Ch09 do not exceed CI abundance). Since silica condenses after pyroxene during fractional condensation (Petaev and Wood 1998), silica-bearing Ch06 may have condensed after porous Ch09, which consists only of low-Ca pyroxene. If the three chondrules formed by fractional condensation, they may have formed in the following order: refractory-rich Ch01 ( $\Delta^{17}\text{O} \sim +2.2$  ‰), porous Ch09 ( $\sim -6$  ‰), and silica-bearing Ch06 ( $\sim -6.4$  ‰).

The CC chondrules from SaU 290 show various degrees of color and optical transparency (Fig. 2). Based on the mineral assemblage, chemistry, and oxygen isotope ratios, the CC chondrules from SaU 290 are classified into four types: typically with  $\Delta^{17}\text{O}$  of -2.2 ‰ (black opaque and white-clouded/transparent), refractory-rich with  $\Delta^{17}\text{O}$  of +2.2 ‰ (black opaque), silica-bearing with  $\Delta^{17}\text{O}$  of -6.4 ‰ (white-clouded/transparent), and porous with  $\Delta^{17}\text{O}$  of -6 ‰ (white-clouded/transparent). Chondrules with various colors are included in the typical type, and there appears to be no relationship between color and classification. The typical chondrules have  $\Delta^{17}\text{O}$  values of -2.2 ‰, while chemically distinct chondrules have distinct  $\Delta^{17}\text{O}$  values. There may be a relationship between chemistry and oxygen isotope ratios, although statistics are still poor. More data will reveal the relationship between chemistry and oxygen isotope ratios for magnesian CC chondrules.

CH chondrites may be related to Stardust particles (see Introduction; Weisberg and Connolly 2008). Here we compare the SaU 290 chondrules and chondrule-like Stardust particles. The  $\Delta^{17}\text{O}$  values of -2.2 ‰ observed from typical CC chondrules in the SaU 290 CH chondrite are identical to  $\Delta^{17}\text{O}$  values of -2 ‰ observed from a majority of chondrule-like Stardust particles (Nakamura et al. 2008a; 2009). However, the latter shows porphyritic texture and the  $\Delta^{17}\text{O}$  values of -2 ‰ were observed in pyroxene grains with Mg# of 96 - 86 (Nakamura et al. 2008a). The CH chondrite chondrules in this study (Fig. 6 and Table 3) are texturally and chemically different from the chondrule-like Stardust particles, and there seems to be no clear relationship between them.

## CONCLUSIONS

We developed new multiple-hole disks (with 7-holes and 3-holes) for high precision stable isotope analyses of tiny particles such as AMMs, IDPs, and Stardust particles using an ion microprobe. Performance tests show that the new multiple-hole disks are applicable to tiny particle analysis as long as the particles are located within the  $\sim 500$   $\mu\text{m}$ -radius of the hole center for 7-hole disks and within the  $\sim 1$  mm-radius of the hole center for 3-hole disks. This requirement is fulfilled by the appropriate sample preparation.

Oxygen three isotope analyses of the magnesian CC chondrules from the SaU 290 CH chondrite showed that most of the chondrules have nearly identical oxygen isotope ratios ( $\Delta^{17}\text{O} = -2.2 \pm 0.6$  ‰; 2SD), which is consistent with those of magnesian CC chondrules in other metal-rich carbonaceous chondrites (Krot et al. 2010). These data support the view that most magnesian CC chondrules in metal-rich carbonaceous chondrites formed by a single impact heating event (Krot et al. 2010). However, the rest of the magnesian CC chondrules from SaU 290 have a wide range of  $\Delta^{17}\text{O}$  values from -6.4 ‰ to +2.2 ‰ that obviously could not be formed by the impact heating event common to other magnesian CC chondrules with  $\Delta^{17}\text{O}$  value of -2.2 ‰. Given that the range of  $\Delta^{17}\text{O}$  values (-6.4 ‰ to +2.2 ‰) is within (similar to) that of the type I porphyritic chondrules in a CH/CB chondrite (Krot et al. 2010), it may be possible that the CC chondrules with distinct  $\Delta^{17}\text{O}$  values formed together with the type I porphyritic chondrules in the solar nebula.

## ACKNOWLEDGEMENTS

The authors are grateful to K. Nagashima and P. R. Heck for their thorough and helpful reviews and A. Ruzicka for thoughtful comments and for handling this paper. The authors also thank M. Kimura for constructive discussion, T. Nakamura and T. Noguchi for their helpful advice for sample preparation and support for SR-XRD, J. Fournelle for calibration and help with SEM and EPMA measurements, J. Kern for SIMS and profilometer support, and the Physical Sciences Laboratory at the University of Wisconsin for fabrication of multiple-hole disks. The bulk sample of SaU 290 was kindly provided from the Bartoschewitz Meteorite Laboratory. This work is supported by the NASA SRLIDAP program (NK, NNX09AC30G) and JSPS Research Fellowships for Young Scientists (DN). WiscSIMS is partly supported by NSF-EAR (0319230, 0744079).

## References

- Anders E. and Grevesse N. 1989. Abundances of the elements: Meteoritic and solar. *Geochimica et Cosmochimica Acta* 53:197-214.
- Clayton R. N., Onuma N., Grossman L., and Mayeda T. K. 1977. Distribution of the pre-solar component in Allende and other carbonaceous chondrites. *Earth and Planetary Science Letters* 34:209-224.
- Clayton R. N., Mayeda T. K., Goswami J. N., and Olsen E. J. 1991. Oxygen isotope studies of ordinary chondrites. *Geochimica et Cosmochimica Acta* 55:2317-2337.
- Floss C., Stadermann F. J., Bradley J. P., Dai Z. R., Bajt S., Graham G., and Lea A. S. 2006. Identification of isotopically primitive interplanetary dust particles: A NanoSIMS isotopic imaging study. *Geochimica et Cosmochimica Acta* 70:2371-2399.
- Greenwood J. P., Rubin A. E., and Wasson J. T. 2000. Oxygen isotopes in R-chondrite magnetite and olivine: links between R chondrites and ordinary chondrites. *Geochimica et Cosmochimica Acta* 64:3897-3911.
- Heck P. R., Ushikubo T., Schmitz B., Kita N. T., Spicuzza M. J., and Valley J. W. 2010. A single

- asteroidal source for extraterrestrial Ordovician chromite grains from Sweden and China: High-precision oxygen three-isotope SIMS analysis. *Geochimica et Cosmochimica Acta* 74:497-509.
- Hezel D. C., Palme H., Brenker F. E., and Nasdala L. 2003. Evidence for fractional condensation and reprocessing at high temperatures in CH chondrites. *Meteoritics & Planetary Science* 38:1199-1215.
- Ivanova M. A., Kononkova N. N., Krot A. N., Greenwood R. C., Franchi I. A., Verchovsky A. B., Trieloff M., Korochantseva E. V., and Brandstätter F. 2008. The Isheyev meteorite: Mineralogy, petrology, bulk chemistry, oxygen, nitrogen, carbon isotopic compositions, and  $^{40}\text{Ar}$ - $^{39}\text{Ar}$  ages. *Meteoritics & Planetary Science* 43:915-940.
- Jones R. H., Guan Y., Leshin L. A., Larsen T., and Sharp Z. D. 2005. Oxygen isotope distribution in NWA 739, a CH chondrite with affinities to Acfer 182 (abstract #1813). 36th Lunar and Planetary Science Conference. CD-ROM.
- Kita N. T., Ushikubo T., Fu B., and Valley J. W. 2009. High precision SIMS oxygen isotope analysis and the effect of sample topography. *Chemical Geology* 264:43-57.
- Kita N. T., Nagahara H., Tachibana S., Tomomura S., Spicuzza M. J., Fournelle J. H., and Valley J. W. 2010. High precision SIMS oxygen three isotope study of chondrules in LL3 chondrites: Role of ambient gas during chondrule formation. *Geochimica et Cosmochimica Acta* 74:6610-6635.
- Krot A. N., Meibom A., and Keil K. 2000. Volatile-poor chondrules in CH carbonaceous chondrites: formation at high ambient nebular temperature (abstract #1418). 31st Lunar and Planetary Science Conference. CD-ROM.
- Krot A. N., Meibom A., Russell S. S., Alexander C. M. O'D., Jeffries T. E., and Keil K. 2001. A new astrophysical setting for chondrule formation. *Science* 291: 1776-1779.
- Krot A. N., Meibom A., Weisberg M. K., and Keil K. 2002. The CR chondrite clan: Implications for early solar system processes. *Meteoritics & Planetary Science* 37:1451-1490.
- Krot A. N., Yurimoto H., McKeegan K. D., Leshin L., Chaussidon M., Libourel G., Yoshitake M., Huss G. R., Guan Y., and Zanda B. 2006. Oxygen isotopic compositions of chondrules: implications for evolution of oxygen isotopic reservoirs in the inner solar nebula. *Chemie der Erde* 66:249-276.



- Krot A. N., Nagashima K., Yoshitake M., and Yurimoto H. 2010. Oxygen isotopic compositions of chondrules from the metal-rich chondrites Isheyevo (CH/CB<sub>b</sub>), MAC 02675 (CB<sub>b</sub>) and QUE 94627 (CB<sub>b</sub>). *Geochimica et Cosmochimica Acta* 74:2190-2211.
- Lofgren G. E. 1996. A dynamic crystallization model for chondrule melts. In *Chondrules and the protoplanetary disk*, edited by Hewins R. H., Jones R. H., and Scott E. R. D. Cambridge: Cambridge University Press. pp. 187-196.
- Messenger S., Keller L. P., Stadermann F. J., Walker R. M., and Zinner E. 2003. Samples of stars beyond the solar system: silicate grains in interplanetary dust. *Science* 300:105-108.
- Messenger S., Keller L. P., and Lauretta D. S. 2005. Supernova olivine from cometary dust. *Science* 309:737-741.
- McKeegan K. D., Aléon J., Bradley J., Brownlee D., Busemann H., Butterworth A., Chaussidon M., Fallon S., Floss C., Gilmour J., Gounelle M., Graham G., Guan Y., Heck P. R., Hoppe P., Hutcheon I. D., Huth J., Ishii H., Ito M., Jacobsen S. B., Kearsley A., Leshin L. A., Liu M.-C., Lyon I., Marhas K., Marty B., Matrajt G., Meibom A., Messenger S., Mostefaoui S., Mukhopadhyay S., Nakamura-Messenger K., Nittler L., Palma R., Pepin R. O., Papanastassiou D. A., Robert F., Schlutter D., Snead C. J., Stadermann F. J., Stroud R., Tsou P., Westphal A., Young E. D., Ziegler K., Zimmermann L., and Zinner E. 2006. Isotopic compositions of cometary matter returned by Stardust. *Science* 314:1724-1728.
- Nakamura T., Noguchi T., Tsuchiyama A., Ushikubo T., Kita N. T., Valley J. W., Zolensky M. E., Kakazu Y., Sakamoto K., Mashio E., Uesugi K., and Nakano T. 2008a. Chondrulelike objects in short-period comet 81P/Wild 2. *Science* 321:1664-1667.
- Nakamura T., Tsuchiyama A., Akaki T., Uesugi K., Nakano T., Takeuchi A., Suzuki Y., and Noguchi T. 2008b. Bulk mineralogy and three-dimensional structures of individual Stardust particles deduced from synchrotron X-ray diffraction and microtomography analysis. *Meteoritics & Planetary Science* 43:247-259.
- Nakamura T., Noguchi T., Tsuchiyama A., Ushikubo T., Kita N. T., Valley J. W., Takahata N., Sano Y.,

- Zolensky M. E., Kakazu Y., Uesugi K., and Nakano T. 2009. Additional Evidence for the Presence of Chondrules in Comet 81P/Wild 2. *Meteoritics & Planetary Science* 44:A153.
- Nakashima D. and Nagao K. 2008. Noble gases in individual glassy spherules from the SaU 290 CH3 chondrite. *Meteoritics & Planetary Science* 43:A112.
- Park J., Okazaki R., Nagao K., Bartoschwitz R., Kusakabe M., and Kimura M. 2005. Noble gases and oxygen isotopes of new CH chondrite, SaU 290 with abundant solar gases (abstract). *Antarctic Meteorites, NIPR, Tokyo* 29:69-70.
- Petaev M. I. and Wood J. A. 1998. The condensation with partial isolation (CWPI) model of condensation in the solar nebula. *Meteoritics & Planetary Science* 33:1123-1137.
- Read W. F. 1986. Possible impact spherules from near the base of the middle Ordovician in northern Illinois. *Meteoritics* 21:251-262.
- Scott E. R. D. 1988. A new kind of primitive chondrite, Allan Hills 85085. *Earth and Planetary Science Letters* 91:1-18.
- Scott E. R. D. and Krot A. N. 2003. Chondrites and their components. In *Meteorites, Comets, and Planets*, vol. 1, edited by A. M. Davis, pp. 143-200. Treatise on Geochemistry, edited by H. D. Holland and K. K. Turekian. Elsevier B. V., Amsterdam.
- Tachibana S., Nagahara H., Mostefaoui S., and Kita N. T. 2003. Correlation between relative ages inferred from  $^{26}\text{Al}$  and bulk compositions of ferromagnesian chondrules in least equilibrated ordinary chondrites. *Meteoritics & Planetary Science* 38:939-962.
- Valley J. W. and Kita N. T. 2009. In situ Oxygen Isotope Geochemistry by Ion Microprobe. Mineralogical Association of Canada Short Course vol. 41:19-63.
- Wasson J. T. 1996. Chondrule formation: Energetics and length scales. In *Chondrules and the Protoplanetary Disk*, edited by Hewins R. H., Jones R. H., and Scott E. R. D. Cambridge: Cambridge University Press. pp. 45-54.
- Weisberg M. K. and Connolly H. C. Jr. 2008. On the relationship between chondrites, comets and asteroids, a petrologic perspective (abstract #1981). 39th Lunar and Planetary Science Conference.

CD-ROM.

- Weisberg M. K., Prinz M., Clayton R. N., Mayeda T. K., Grady M. M., and Pillinger C. T. 1995. The CR chondrite clan. *Proceedings of the NIPR Symposium on Antarctic Meteorites* 8:11-32.
- Weisberg M. K., Ebel D. S., Kimura M., Kita N. T., and Nakashima D. 2010. Petrology and oxygen isotopes of chondrules in the Kota Kota EH3 chondrite. (abstract #1533). 41st Lunar and Planetary Science Conference. CD-ROM.
- Yada T., Floss C., Stadermann F. J., Zinner E., Nakamura T., Noguchi T., and Lea A. S. 2008. Stardust in Antarctic micrometeorites. *Meteoritics & Planetary Science* 43:1287-1298.
- Yoshitake M. and Yurimoto H. 2004. Oxygen isotopic distributions among chondrules in Acfer 214, CH chondrite. In *Chondrites and Protoplanetary Disk*: Lunar and Planetary Institute, Houston. Abstract #9049.
- Young E. D. and Russell S. S. 1998. Oxygen reservoirs in the early solar nebula inferred from an Allende CAI. *Science* 282:452-455.
- Yurimoto H., Krot A. N., Choi B-G, Aléon J., Kunihiro T., and Brearley A. J. 2008. Oxygen isotopes of chondritic components. *Reviews in Mineralogy & Geochemistry* 68:141-186.
- Zolensky M. E., Zega T. J., Yano H., Wirick S., Westphal A. J., Weisberg M. K., Weber I., Warren J. L., Velbel M. A., Tsuchiyama A., Tsou P., Toppani A., Tomioka N., Tomeoka K., Teslich N., Taheri M., Susini J., Stroud R., Stephan T., Stadermann F. J., Snead C. J., Simon S. B., Simionovici A., See T. H., Robert F., Rietmeijer F. J. M., Rao W., Perronnet M. C., Papanastassiou D. A., Okudaira K., Ohsumi K., Ohnishi I., Nakamura-Messenger K., Nakamura T., Mostefaoui S., Mikouchi T., Meibom A., Matrajt G., Marcus M. A., Leroux H., Lemelle L., Le L., Lanzirotti A., Langenhorst F., Krot A. N., Keller L. P., Kearsley A. T., Joswiak D., Jacob D., Ishii H., Harvey R., Hagiya K., Grossman L., Grossman J. N., Graham G. A., Gounelle M., Gillet P., Genge M. J., Flynn G., Ferroir T., Fallon S., Ebel D. S., Dai Z. R., Cordier P., Clark B., Chi M., Butterworth A. L., Brownlee D. E., Bridges J. C., Brennan S., Brearley A., Bradley J. P., Bleuet P., Bland P. A. and Bastien R. 2006. Mineralogy and petrology of comet 81P/Wild 2 nucleus samples. *Science* 314:1735–1739.

## Figure captions

**Fig. 1:** A photograph of the 7-hole disk (disk-1) mounted in the CAMECA holder (a), a photograph of the 3-hole disk (disk-3), schematic illustrations showing mounting an epoxy disk in the 7-hole disk (c) and epoxy disk preparation procedures (d). In panel (c), an upper disk without a tungsten lip is depicted (WiscSIMS design), while that used in Nakamura et al. (2008a) has a tungsten lip.

**Fig. 2:** A photomicrograph of the >300 chondrules extracted from the SaU 290 CH chondrite.

**Fig. 3:** Values of  $\delta^{18}\text{O}$  at outer holes relative to the bracketing analyses at the center hole in the 7-hole disks (a, the disk-1; b, the disk-2). The error bars are internal error from counting statistics (2SE).

**Fig. 4:** Values of  $\delta^{18}\text{O}$  at two south holes relative to the bracketing analyses at the north hole in the 3-hole disks (a, the disk-3; b, the disk-4). The error bars are internal error from counting statistics (2SE).

**Fig. 5:** Contour maps of all combined  $\delta^{18}\text{O}$  values of different locations relative to the bracketing analyses at the center of the grains in individual holes in the 7-hole disks (a) and in the 3-hole disks (b). Contour interval is 0.25 ‰. Small open circles indicate locations where oxygen two isotopes were analyzed (56 spots in the 7-hole disks and 80 spots in the 3-hole disks).

**Fig. 6:** BSE images of polished surfaces of the SaU 290 chondrules. In panel b, a brighter grain next to the chondrule Ch02 is San Carlos olivine. In panel d, three holes in the chondrule Ch05 are pits made by oxygen isotope analyses with 15  $\mu\text{m}$  spots. In panel f, white dots scattering on the chondrule surface are Fe-metal grains (< 1  $\mu\text{m}$  in diameter; detected by SEM-EDS). In panel h, there appears to be a dark rim surrounding the porous interior. This is just due to an inclined periphery and is not a feature of the chondrule. Oval regions with white circles outline pits from oxygen isotope measurements (Ch09 was not analyzed with 15  $\mu\text{m}$  spots).

**Fig. 7:** Enlarged BSE images of the SaU 290 chondrules. In panel b, white dots scattering on the chondrule surface are Fe-metal grains (< 1  $\mu\text{m}$  in diameter; identified by SEM-EDS). White-outlined ovals represent the primary beam size of 3  $\times$  4  $\mu\text{m}$  for reference, but do not indicate sputtered areas. The ellipses in panels a and d indicate mineral phases but not locations of oxygen isotope analyses.

Abbreviations: Hpx, high-Ca pyroxene; Lpx, low-Ca pyroxene; glass, feldspathic glass; Wo5, one of two types of low-Ca pyroxene (En94Wo5) in Ch06; Wo1, one of two types of low-Ca pyroxene (En98Wo1) in Ch06; Cr, cristobalite.

**Fig. 8:** Synchrotron radiation X-ray diffraction patterns of the SaU 290 chondrules in a range of diffraction angles ( $2\theta$ ) from 4 to 62 °.

**Fig. 9:** Defocused-beam ( $\sim 25 \mu\text{m}$ ) electron microprobe analyses of the SaU 290 chondrules in terms of atomic ratios of Al, (Mg+Fe), and Si. Also shown are stoichiometric olivine, low-Ca pyroxene, feldspar (anorthite, albite, and orthoclase), and silica.

**Fig. 10:** Bulk chemical compositions (by defocused-beam EPMA) of the SaU 290 chondrules normalized by Si and elemental abundance of CI chondrites (Anders and Grevesse 1989) in linear scale. The dotted area represents a field of bulk chemical compositions of CC chondrules in other CH chondrites (Krot et al. 2000).

**Fig. 11:** Relative  $\delta^{18}\text{O}$  and  $\delta^{17}\text{O}$  values of outer SC-Ol grains from the analyses at the center SC-Ol grain (disk-1). In individual holes, the SC-Ol grains were used as running standards bracketing chondrule analyses. Error bars are external reproducibility (2SD). TF represents the terrestrial fractionation line.

**Fig. 12:** Oxygen isotope ratios of the SaU 290 chondrules analyzed with 15  $\mu\text{m}$  spots (a) and with 4  $\mu\text{m}$  spots (b). TF, Y&R, and CCAM represent the terrestrial fractionation line, the Young & Russell line (Young and Russell 1998), and the carbonaceous chondrite anhydrous mineral line (Clayton et al. 1977). Oxygen isotope ratios of the bulk meteorite are from Park et al. (2005).

**Fig. 13:** Oxygen isotope ratios of the SaU 290 chondrules are plotted as deviations from the terrestrial fractionation (TF) line ( $\Delta^{17}\text{O} = \delta^{17}\text{O} - 0.52 \times \delta^{18}\text{O}$ ).

Table 1. Measured $\delta^{18}\text{O}$ values relative to SC-OI grain in the center hole*					
disk-1	$\delta^{18}\text{O} \pm 2\text{SE} (\text{‰})$		disk-2	$\delta^{18}\text{O} \pm 2\text{SE} (\text{‰})$	
NW	0.51	0.37	W	0.08	0.32
	0.42	0.38		-0.14	0.33
	0.32	0.38		0.05	0.32
	<b>0.42</b>	<b>0.19</b>		-0.15	0.27
			<b>-0.04</b>	<b>0.25</b>	
W	-0.31	0.41	NW	-0.39	0.27
	-0.51	0.38		-0.38	0.31
	-0.49	0.39		-0.51	0.31
	<b>-0.44</b>	<b>0.22</b>		-0.54	0.31
			<b>-0.46</b>	<b>0.16</b>	
NE	0.71	0.39	NE	-0.34	0.28
	0.53	0.41		-0.33	0.26
	-0.07	0.41		-0.38	0.31
	<b>0.39</b>	<b>0.82</b>		-0.47	0.32
			<b>-0.38</b>	<b>0.13</b>	
E	0.85	0.32	E	-0.19	0.27
	0.46	0.32		-0.10	0.30
	0.55	0.39		-0.20	0.29
	<b>0.62</b>	<b>0.41</b>		-0.22	0.33
			<b>-0.18</b>	<b>0.11</b>	
SW	-0.41	0.37	SE	0.26	0.31
	-0.63	0.38		0.17	0.27
	-0.82	0.39		0.13	0.27
	<b>-0.62</b>	<b>0.41</b>		-0.03	0.25
			<b>0.13</b>	<b>0.25</b>	
SE	0.04	0.33	SW	-0.35	0.29
	-0.28	0.39		-0.42	0.30
	-0.22	0.41		-0.59	0.33
	<b>-0.16</b>	<b>0.34</b>		-0.38	0.32
			<b>-0.43</b>	<b>0.22</b>	
Center		<b>0.3</b>	Center		<b>0.22</b>

\*Bold-faced numbers are average values and external reproducibility (2SD).

Table 2. Measured  $\delta^{18}\text{O}$  values relative to SC-OI grain in the north hole\*

disk-3	$\delta^{18}\text{O} \pm 2\text{SE} (\text{‰})$		disk-4	$\delta^{18}\text{O} \pm 2\text{SE} (\text{‰})$	
	-0.08	0.22		-0.61	0.32
	0.00	0.23		-0.62	0.29
SW	0.06	0.21	SW	-0.88	0.29
	-0.03	0.24		-0.70	0.27
	<b>-0.02</b>	<b>0.12</b>		<b>-0.70</b>	<b>0.24</b>
	-0.31	0.22		0.46	0.31
	-0.42	0.23		0.07	0.27
SE	-0.39	0.22	SE	0.01	0.28
	-0.65	0.23		0.04	0.34
	<b>-0.44</b>	<b>0.29</b>		<b>0.15</b>	<b>0.43</b>

\*Bold-faced numbers are average values and external reproducibility (2SD).

Table 3. Averaged major elemental compositions of the SaU 290 chondrules obtained by defocused-beam electron microprobe analyses and transparency of the chondrules								
chd#	Ch01	Ch02	Ch04	Ch05	Ch06	Ch07	Ch08	Ch09*
Number of Analyses	n=22	n=25	n=8	n=5	n=9	n=8	n=4	n=1
SiO <sub>2</sub>	55.3	55.1	54.0	56.0	62.7	53.7	55.4	55.0
TiO <sub>2</sub>	0.27	0.08	0.08	bdl	0.16	0.07	bdl	0.32
Al <sub>2</sub> O <sub>3</sub>	6.08	1.35	1.07	0.17	3.82	1.25	0.55	3.30
Cr <sub>2</sub> O <sub>3</sub>	0.57	0.70	0.70	0.60	0.71	0.72	0.80	0.60
FeO	0.69	0.32	0.46	0.14	0.40	1.09	0.24	0.45
MnO	0.24	0.11	0.11	bdl	0.26	bdl	0.12	0.21
MgO	31.6	41.2	41.9	42.2	27.2	41.6	41.4	35.0
CaO	3.91	1.24	0.91	0.12	2.59	1.14	0.45	2.38
NiO	bdl	bdl	bdl	bdl	bdl	bdl	bdl	bdl
Na <sub>2</sub> O	1.07	bdl	bdl	bdl	0.60	bdl	bdl	bdl
K <sub>2</sub> O	0.39	bdl	bdl	bdl	0.20	bdl	bdl	bdl
SO <sub>3</sub>	0.07	bdl	bdl	bdl	bdl	bdl	bdl	bdl
Total	100.2	100.1	99.3	99.3	98.7	99.7	99.0	97.4
Mg <sup>#</sup>	98.7	99.8	99.6	99.8	99.0	98.9	99.7	
Transparency <sup>#</sup>	Op	Op	Wh/Tr	Wh/Tr	Wh/Tr	Op	Wh/Tr	Wh/Tr
* Broad beam EPMA data for Ch09 were not available, because of high porosity of Ch09. Instead, focused beam EPMA data with highest analytical total are listed, because analytical totals of other EPMA data are low due to high porosity (81-97 wt%).								
bdl = below detection limit.								
<sup>#</sup> Transparency under an optical microscope. Abbreviations: Op, black opaque; Wh/Tr, white-clouded/transparent.								



Table 4. Averaged major elemental compositions of individual mineral phases in the SaU 290 chondrules obtained by focused-beam electron microprobe analyses.

chd#	Ch01			Ch02		Ch06		
	Low-Ca px	High-Ca px	Glass	Dark	Bright	Low-Ca px		Silica
						Wo1*	Wo5*	
Number of analyses	n=3	n=3	n=3	n=3	n=3	n=3	n=5	n=4
SiO <sub>2</sub>	50.73	53.28	54.20	52.76	53.75	59.55	60.23	79.41
TiO <sub>2</sub>	0.19	0.45	bdl	0.07	0.10	0.16	0.22	0.07
Al <sub>2</sub> O <sub>3</sub>	3.49	5.45	5.99	1.25	1.34	1.26	2.51	2.39
Cr <sub>2</sub> O <sub>3</sub>	0.61	0.80	bdl	0.39	0.71	0.64	0.75	0.22
FeO	0.87	0.72	0.67	0.21	0.27	0.48	0.66	0.18
MnO	0.31	0.29	0.27	bdl	0.06	0.19	0.32	0.08
MgO	42.64	27.12	32.93	42.88	41.46	36.35	32.78	8.86
CaO	1.88	11.04	3.06	0.66	0.94	0.59	2.59	1.21
Na <sub>2</sub> O	0.34	0.27	1.04	bdl	bdl	bdl	0.07	0.41
K <sub>2</sub> O	bdl	bdl	0.43	bdl	bdl	bdl	bdl	0.11
Total	101.06	99.43	98.59	98.30	98.61	99.23	100.12	92.95

bdl = below detection limit.

\* See Fig. 7.

Table 5. Oxygen isotope ratios of the SaU 290 chondrules measured with 15  $\mu\text{m}$  spots, using the 7-hole disk (disk-1) and IMS-1280 SIMS\*

	$\delta^{18}\text{O}_{\text{VSMOW}} \pm 2\text{SD} (\text{‰})$		$\delta^{17}\text{O}_{\text{VSMOW}} \pm 2\text{SD} (\text{‰})$		$\Delta^{17}\text{O} \pm 2\text{SD} (\text{‰})$	
Ch01	7.03	0.37	5.62	0.86	1.96	0.77
	7.40	0.37	5.94	0.86	2.09	0.77
	7.05	0.37	6.09	0.86	2.42	0.77
Ch02	0.97	0.74	-1.81	0.53	-2.31	0.55
	0.75	0.74	-1.98	0.53	-2.36	0.55
	0.75	0.74	-1.68	0.53	-2.07	0.55
Ch04	0.01	0.20	-2.20	0.56	-2.21	0.52
	-0.33	0.20	-2.27	0.56	-2.10	0.52
	0.41	0.20	-2.55	0.56	-2.77	0.52
Ch05	0.51	0.81	-1.81	0.69	-2.07	0.82
	0.76	0.81	-1.64	0.69	-2.03	0.82
	0.57	0.81	-1.55	0.69	-1.84	0.82
Ch06 <sup>#</sup>	-6.19	0.46	-9.07	0.65	-5.85	0.55
	-6.64	0.46	-10.18	0.65	-6.73	0.55
	-6.14	0.46	-9.95	0.65	-6.76	0.55
Ch07	0.64	1.85	-2.17	1.60	-2.50	0.85
	0.87	1.85	-2.28	1.60	-2.73	0.85
	0.81	1.85	-1.37	1.60	-1.79	0.85
Ch08	0.20	0.71	-2.36	0.88	-2.46	0.73
	0.14	0.71	-1.75	0.88	-1.83	0.73
	0.11	0.71	-2.54	0.88	-2.60	0.73

\*The uncertainties associated with isotope ratios are external reproducibility (2SD) of six to eight sets of bracketing analyses of San Carlos olivine standard grains.

<sup>#</sup>For Ch06 containing silica, instrumental bias was corrected as a mixture of low Ca pyroxene and silica (14 %), which resulted in  $\delta^{18}\text{O}$  shift of -1.1 ‰ in the bias correction factor compared to low Ca-pyroxene.

Table 6. Oxygen isotope ratios of pyroxene grains in the SaU 290 chondrules measured with 4  $\mu$  m spots, using the 7-hole disk (disk-1) and IMS 1280-SIMS<sup>\*,#</sup>

	$\delta^{18}\text{O}_{\text{VSMOW}} \pm 2\text{SD} (\text{‰})$		$\delta^{17}\text{O}_{\text{VSMOW}} \pm 2\text{SD} (\text{‰})$		$\Delta^{17}\text{O} \pm 2\text{SD} (\text{‰})$		Remarks <sup>S</sup>
Ch01	8.98	0.70	6.60	0.98	1.93	0.87	low-Ca px
	8.11	0.70	5.60	0.98	1.38	0.87	low-Ca px
	8.25	0.70	5.60	0.98	1.31	0.87	high-Ca px
	7.78	0.70	5.80	0.98	1.75	0.87	high-Ca px
	7.96	0.70	6.72	0.98	2.58	0.87	high-Ca px
Ch02	0.83	0.66	-1.22	0.72	-1.65	0.89	brighter phase
	1.58	0.66	-2.60	0.72	-3.42	0.89	brighter phase
	1.26	0.66	-1.31	0.72	-1.96	0.89	darker phase
	1.12	0.66	-2.33	0.72	-2.91	0.89	darker phase
	1.51	0.66	-1.17	0.72	-1.96	0.89	darker phase
Ch04	1.36	0.87	-1.36	0.83	-2.07	0.74	
	1.22	0.87	-0.94	0.83	-1.57	0.74	
	0.36	0.87	-1.05	0.83	-1.24	0.74	
	0.88	0.87	-1.55	0.83	-2.00	0.74	
	1.90	0.87	-1.10	0.83	-2.08	0.74	
Ch06	-5.75	1.77	-9.27	1.58	-6.28	1.05	Wo5
	-6.64	1.77	-9.57	1.58	-6.12	1.05	Wo5
	-6.03	1.77	-9.82	1.58	-6.68	1.05	Wo1
	-8.51	1.77	-11.15	1.58	-6.73	1.05	Wo1
	-8.57	1.77	-10.04	1.58	-5.58	1.05	Wo1
	-10.90	1.77	-12.53	1.58	-6.86	1.05	Wo5
	-7.66	1.77	-10.81	1.58	-6.83	1.05	Wo5
	-11.05	1.77	-12.44	1.58	-6.69	1.05	Wo1

\*Ch09 was also analyzed with 4  $\mu$  m spots, but the  $^{16}\text{O}$  count rates were only 60 % of the SC-O1 grain and other chondrules. Therefore, we decided the Ch09 data were unreliable and do not list in the table. Instead, Ch09 data is listed in online supplements.

<sup>#</sup>The uncertainties associated with isotope ratios are external reproducibility (2SD) of six sets of bracketing analyses of San Carlos olivine standard grains.

<sup>S</sup>See Fig. 7.

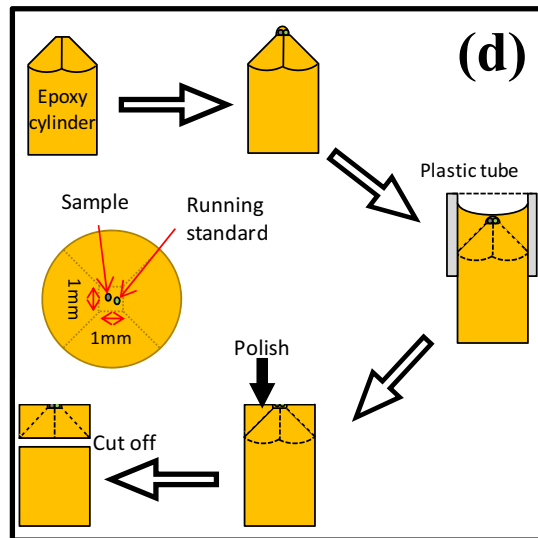
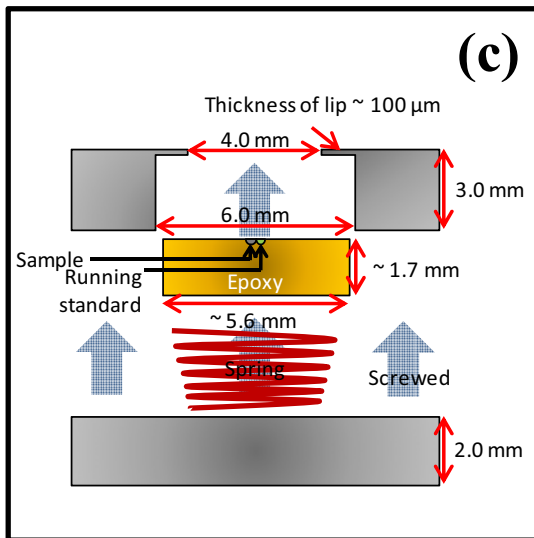
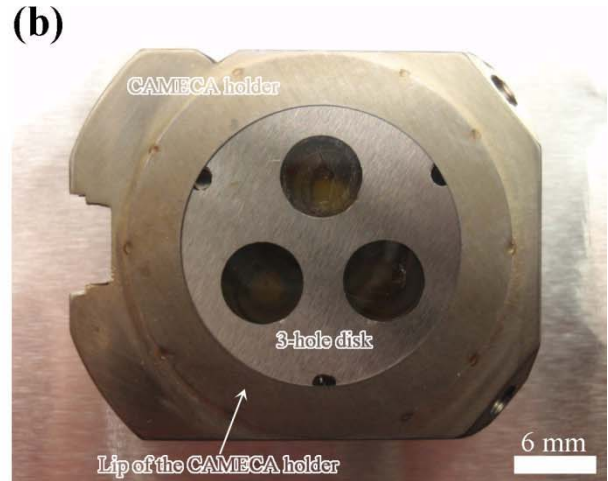
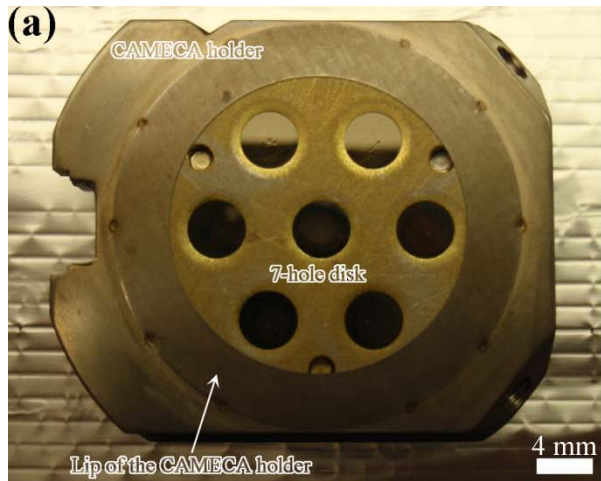


**Fig. 1: Nakashima et al. 2010**

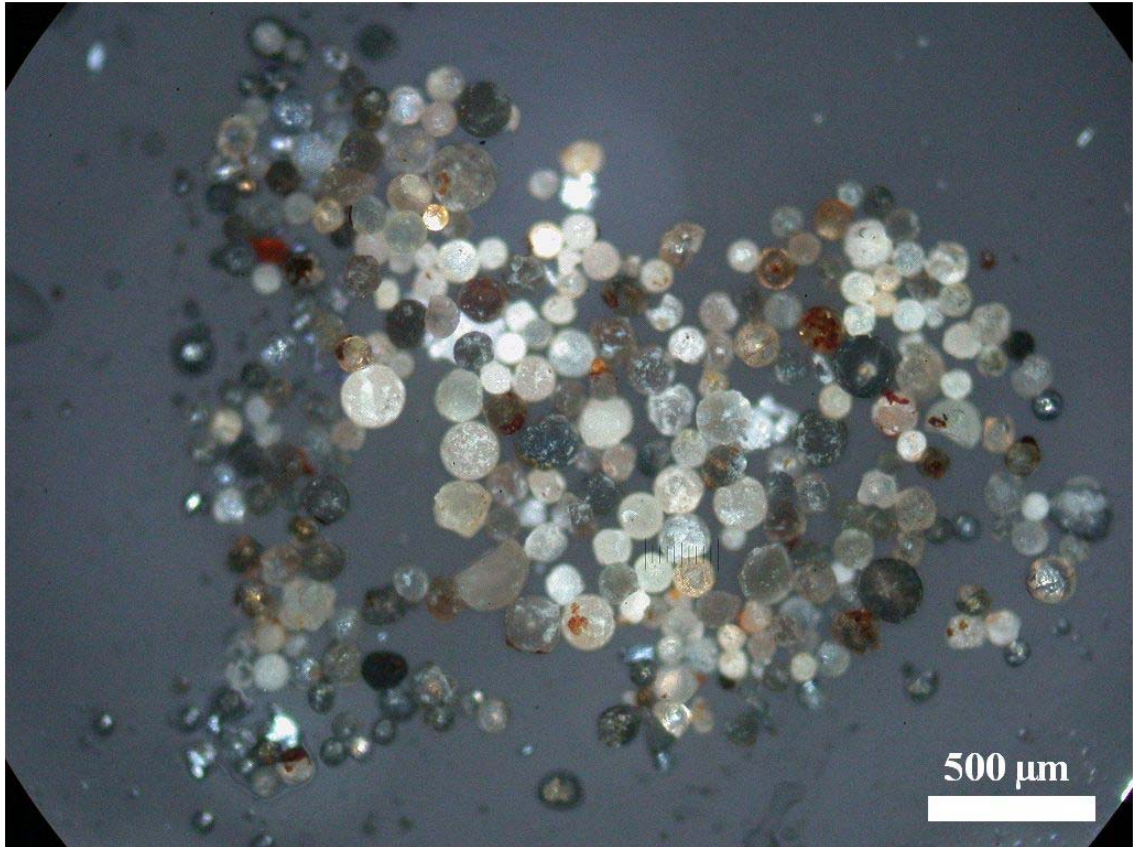


**Fig. 2: Nakashima et al. 2010**

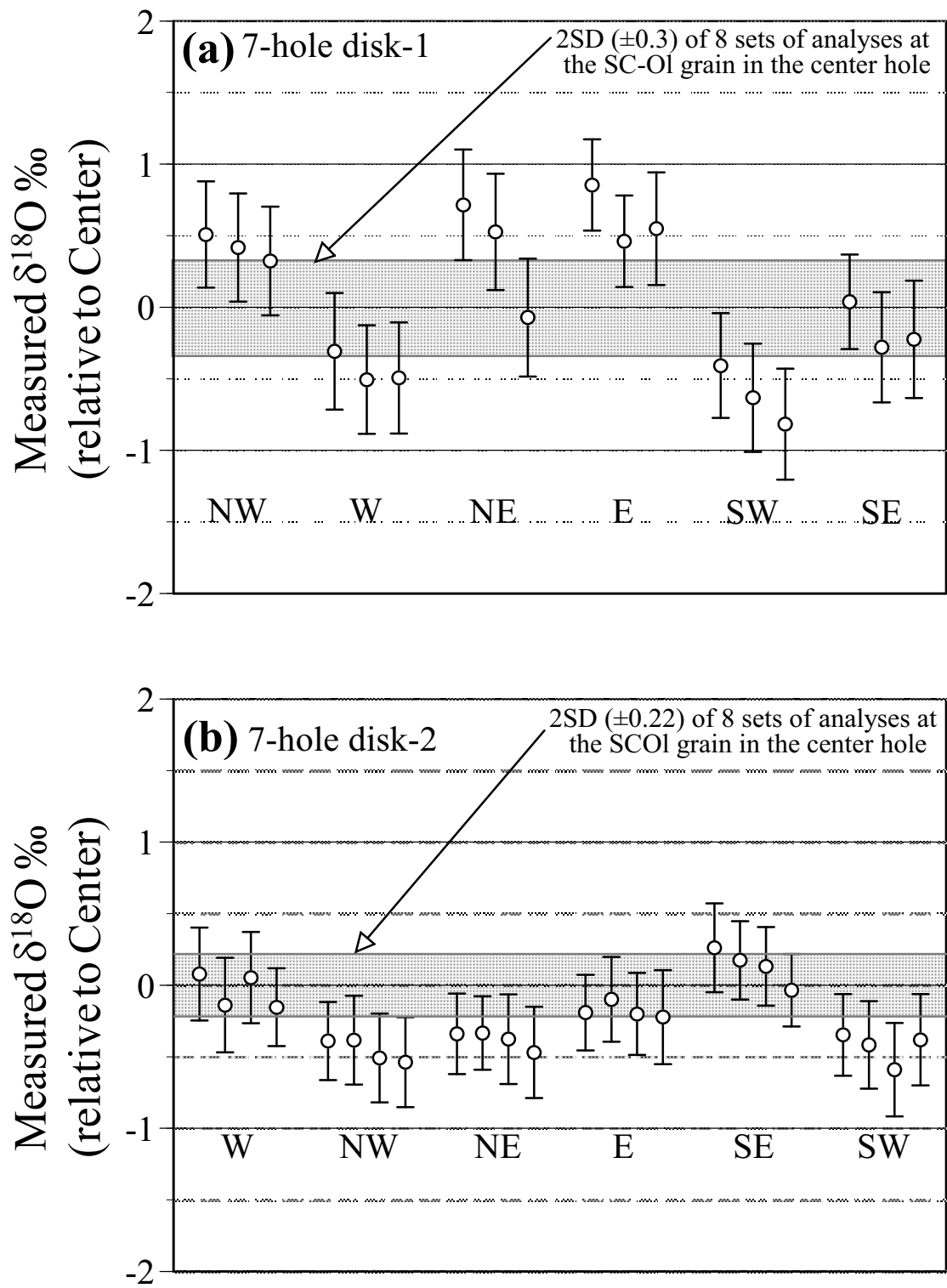


**Fig. 3: Nakashima et al. 2010**

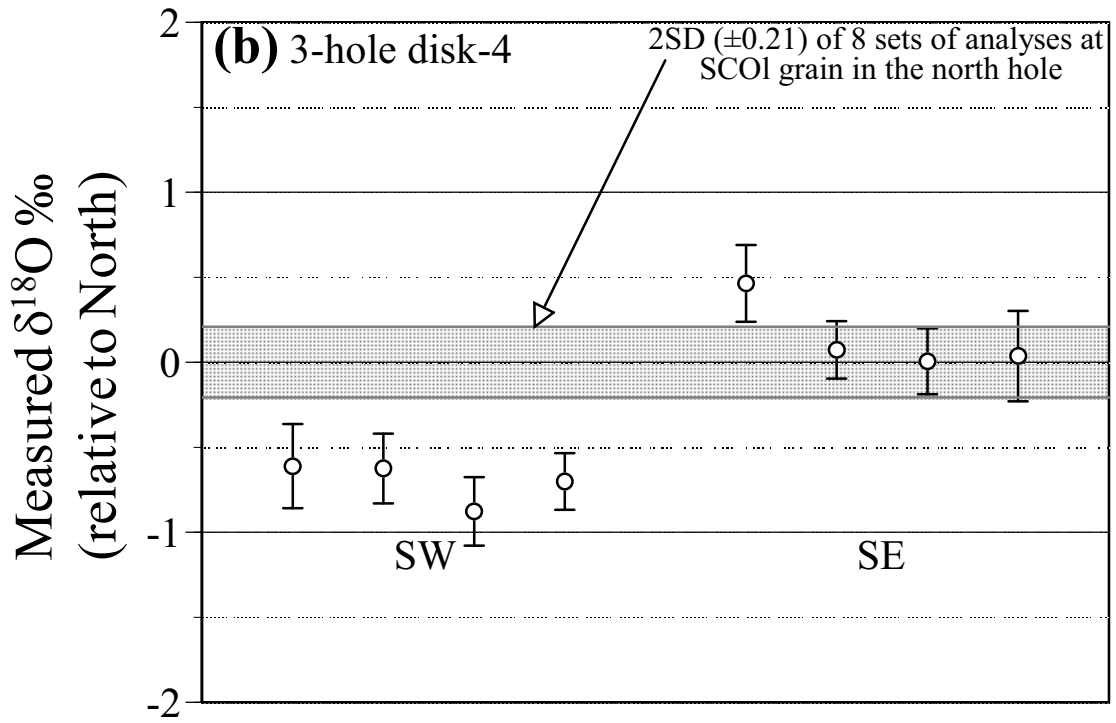
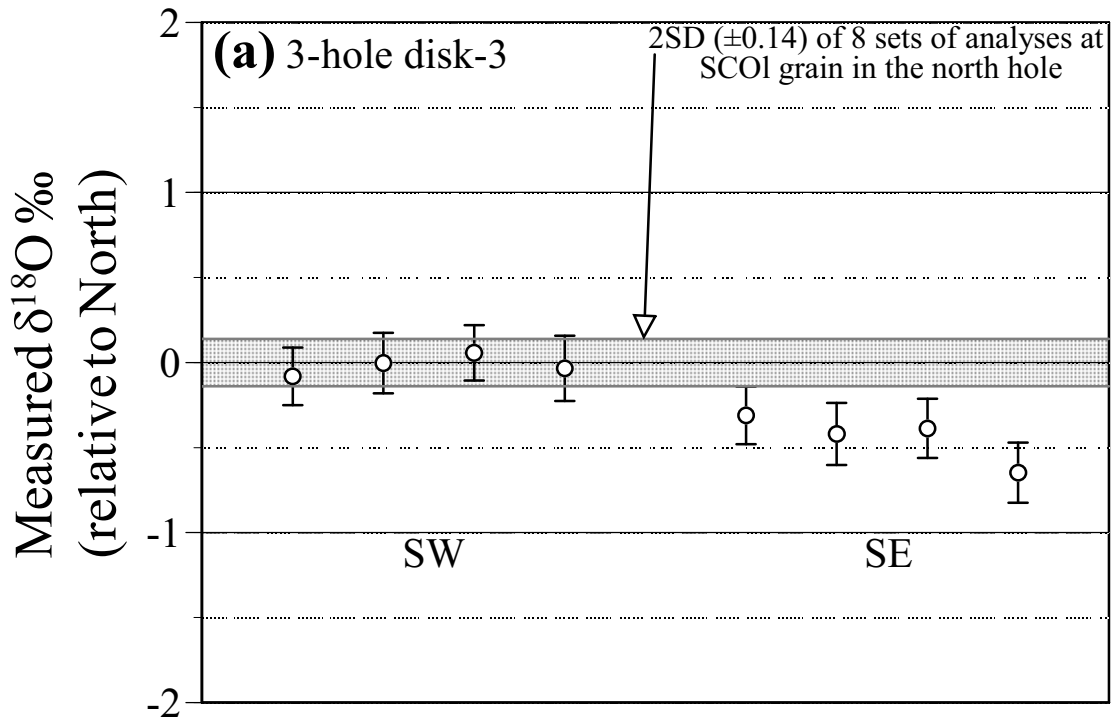


**Fig. 4: Nakashima et al. 2010**

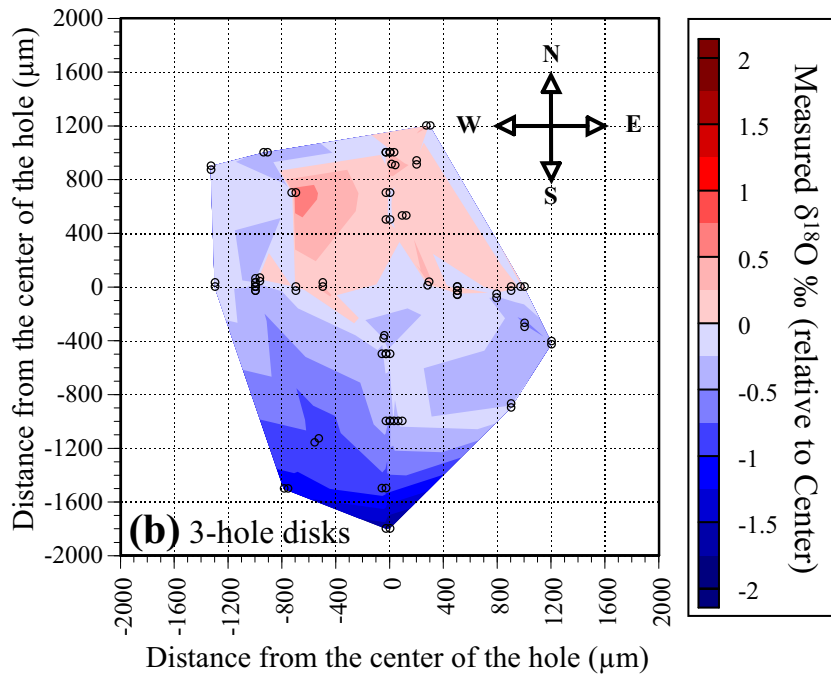
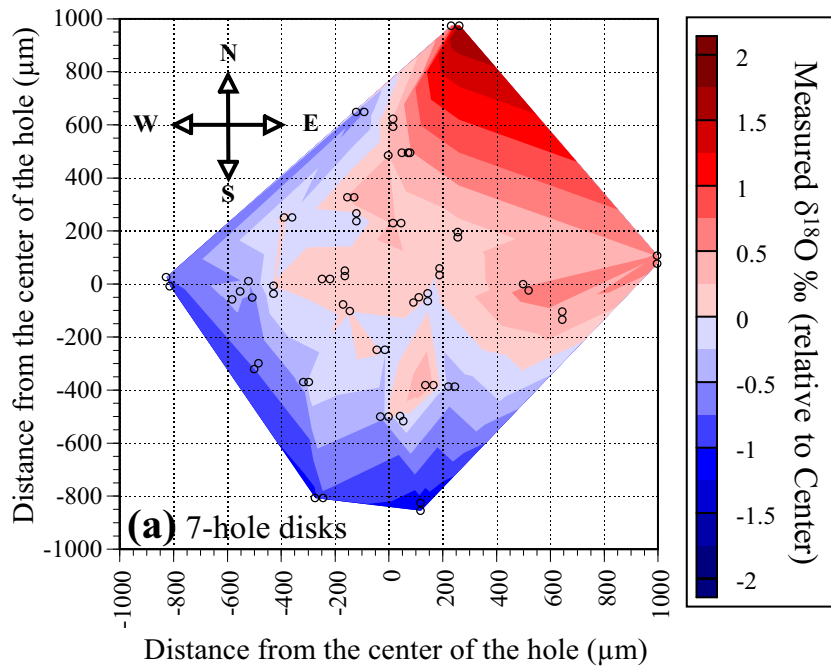


**Fig. 5: Nakashima et al. 2010**



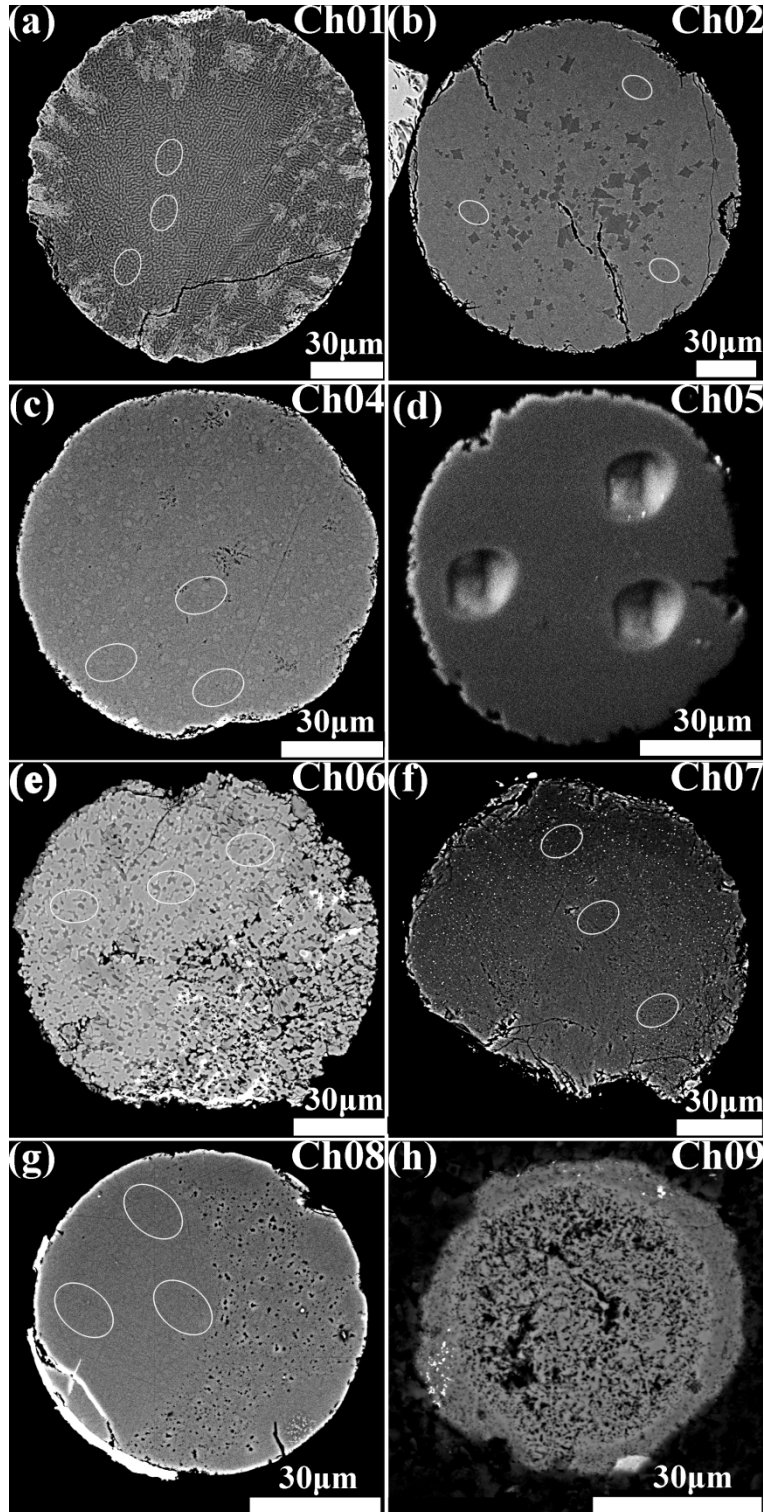


**Fig. 6: Nakashima et al. 2010**

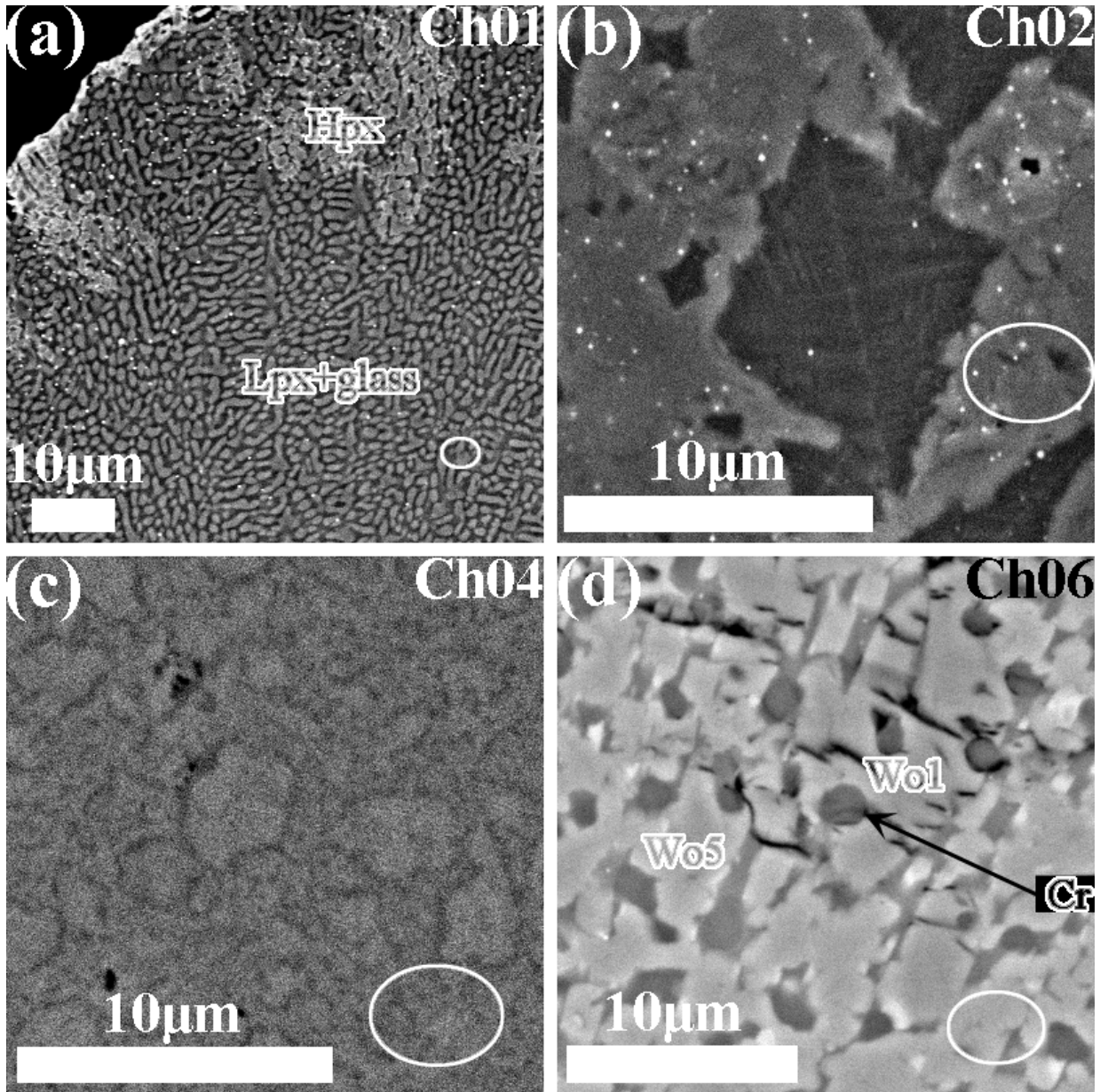


**Fig. 7: Nakashima et al. 2010**

Ol: Olivine  
 Px: low-Ca pyroxene  
 Cr: Cristobalite  
 Un: a phase unidentified

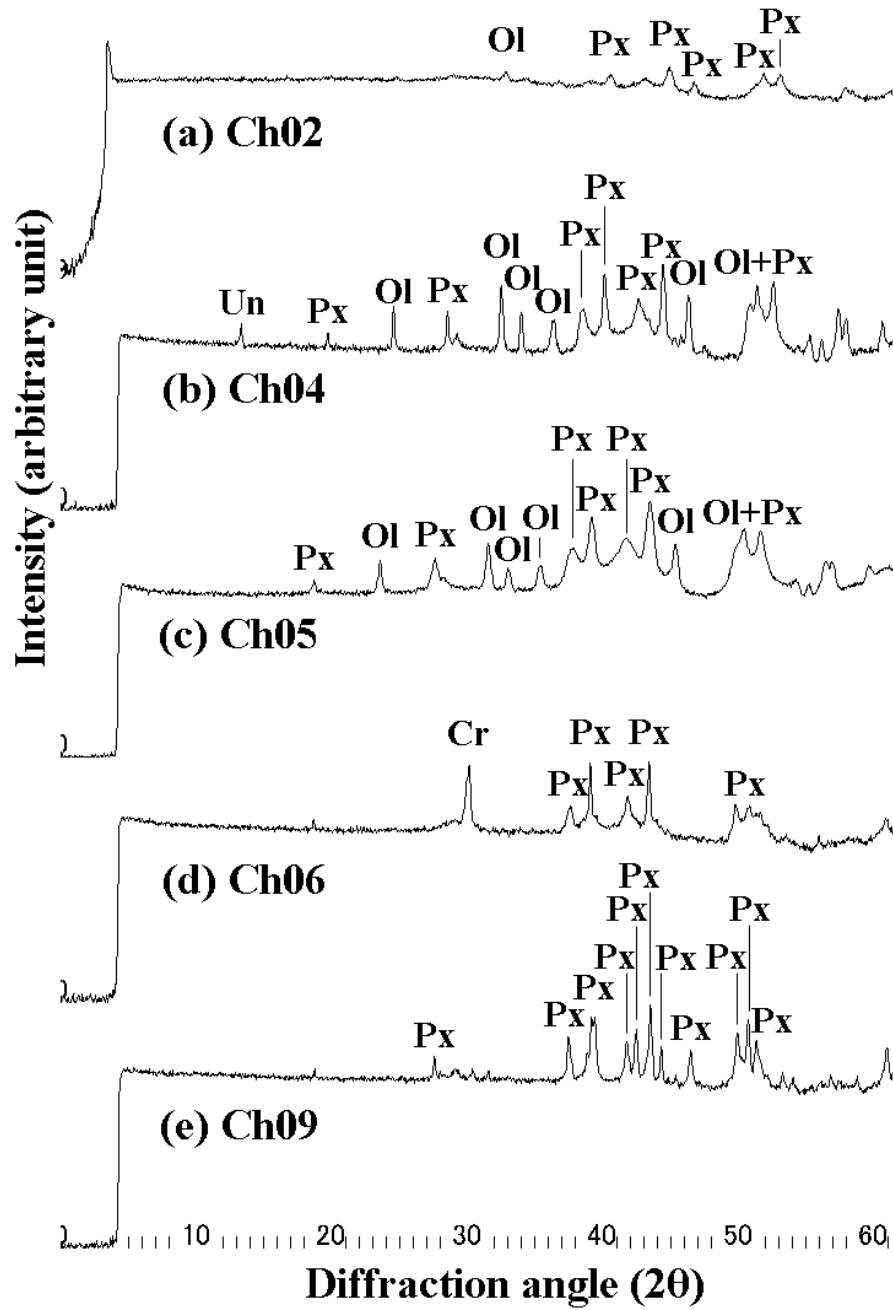


**Fig. 8: Nakashima et al. 2010**

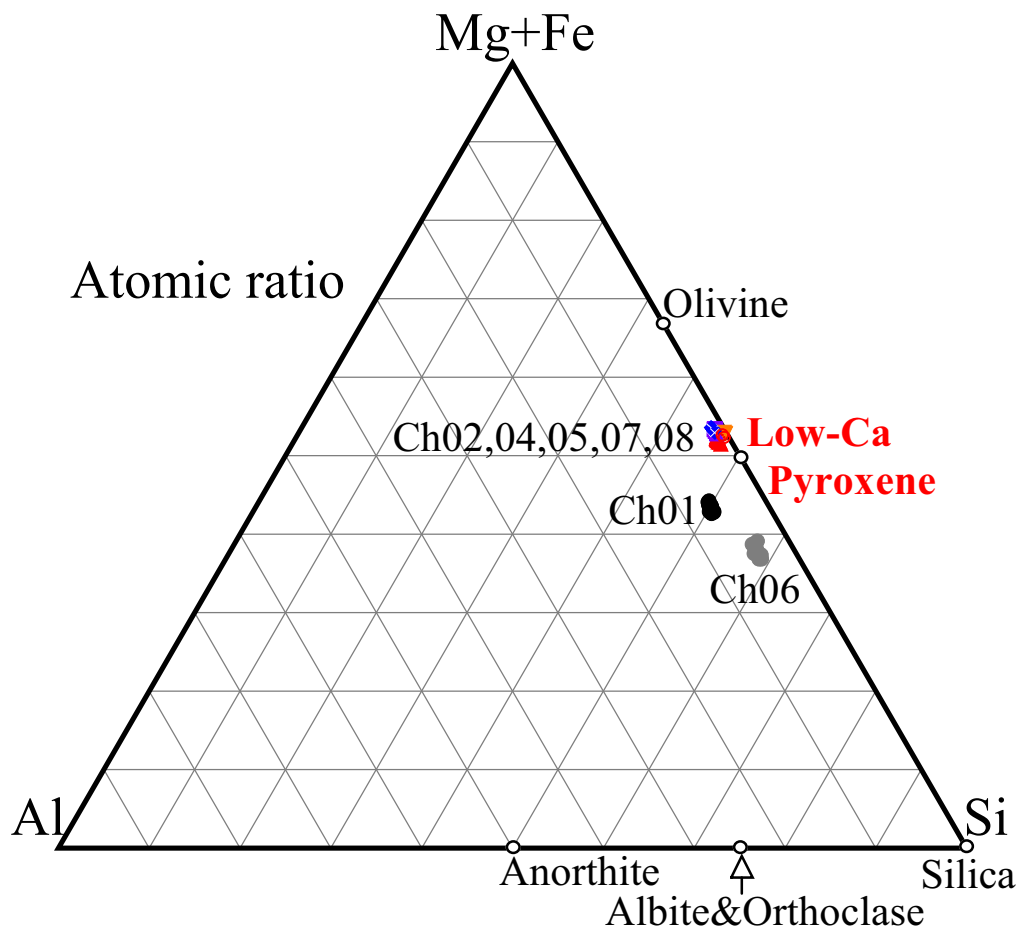


**Fig. 9: Nakashima et al. 2010**

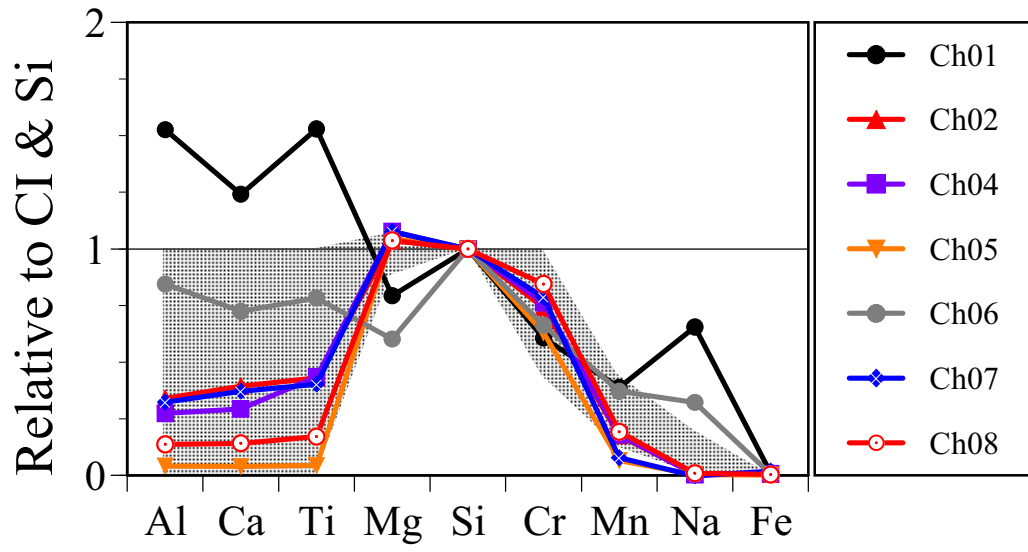


**Fig. 10: Nakashima et al. 2010**



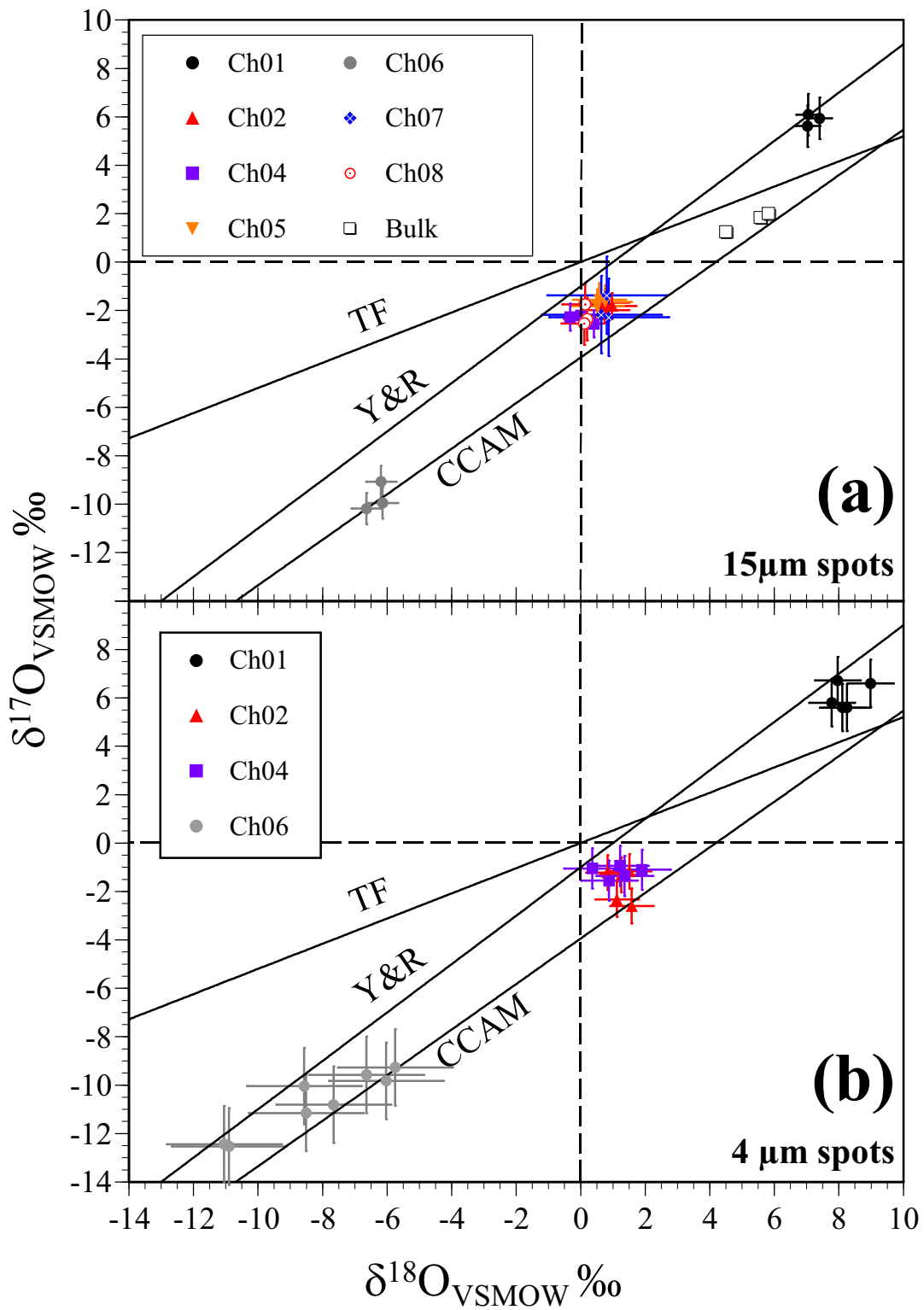


**Fig. 12: Nakashima et al. 2010**

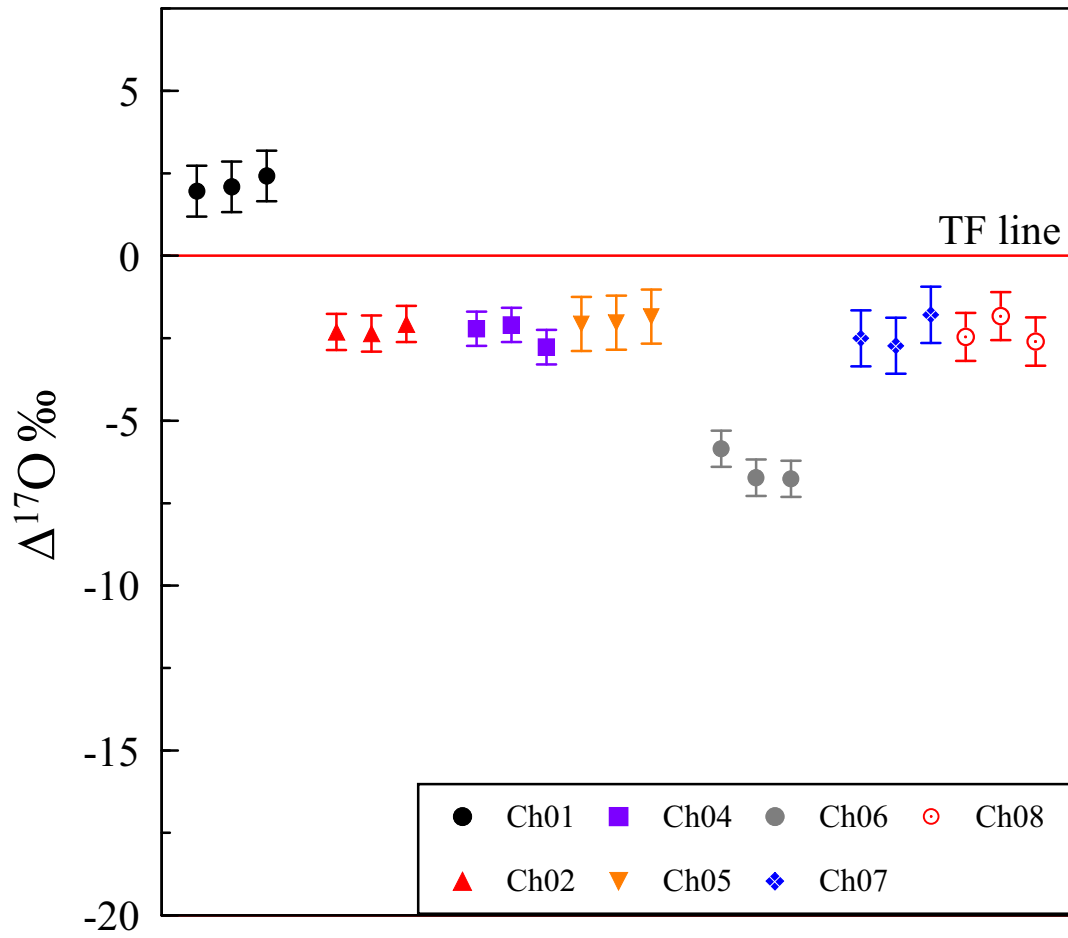


**Fig. 13: Nakashima et al. 2010**



Table A1. Measured  $\delta^{18}\text{O}$  values relative to the center of the grains in individual holes in the 7-hole disk-1\*

Disk-1	$\delta^{18}\text{O} \pm 2\text{SE}$ (‰)	$\Delta X$ $\Delta Y$		
		(μm)		
S	-0.38	0.39	247	-387
	-0.30	0.37	223	-387
	<b>-0.34</b>	<b>0.11</b>		
E	0.03	0.41	190	59
	0.04	0.37	190	34
	<b>0.04</b>	<b>0.02</b>		
Center (±0.32; 2SD)	0.07	0.38	-169	-77
	0.00	0.38	-144	-102
	<b>0.04</b>	<b>0.09</b>		
N	0.27	0.40	-153	327
	0.51	0.38	-128	327
	<b>0.39</b>	<b>0.34</b>		
S	-0.11	0.30	-296	-370
	-0.45	0.33	-316	-370
	<b>-0.28</b>	<b>0.48</b>		
W	0.15	0.32	-162	50
	0.21	0.32	-162	30
	<b>0.18</b>	<b>0.08</b>		
West (±0.21; 2SD)	0.15	0.28	258	196
	0.13	0.34	258	176
	<b>0.14</b>	<b>0.02</b>		
E	0.16	0.29	113	-50
	0.11	0.29	93	-70
	<b>0.14</b>	<b>0.07</b>		

\*Bold-faced numbers are average values and external reproducibility (2SD).

Table A2. Measured  $\delta^{18}\text{O}$  values relative to the center of the grains in individual holes in the 7-hole disk-2\*

Disk-2	$\delta^{18}\text{O} \pm 2\text{SE}$ (‰)		$\Delta X$	$\Delta Y$	
			(μm)		
		0.02	0.32	-427	-7
W 500μm		-0.06	0.31	-427	-37
		<b>-0.02</b>	<b>0.11</b>		
E 150μm		-0.08	0.31	146	-35
		-0.06	0.33	146	-65
		<b>-0.07</b>	<b>0.02</b>		
Center (±0.23; 2SD)	S 250μm	-0.23	0.33	-13	-248
		0.04	0.28	-43	-248
		<b>-0.09</b>	<b>0.39</b>		
N 500μm		0.05	0.33	-388	251
		-0.20	0.32	-358	251
		<b>-0.07</b>	<b>0.35</b>		
W 500μm		0.21	0.47	-247	19
		-0.01	0.47	-217	19
		<b>0.10</b>	<b>0.31</b>		
E 1000μm		0.58	0.45	998	77
		0.51	0.49	998	107
		<b>0.54</b>	<b>0.10</b>		
Northwest (±0.42; 2SD)	N 500μm	-0.60	0.46	-120	649
		-0.44	0.51	-90	649
		<b>-0.52</b>	<b>0.23</b>		
S 500μm		0.46	0.47	137	-381
		0.21	0.46	167	-381
		<b>0.34</b>	<b>0.35</b>		
W 500μm		-0.44	0.49	-581	-58
		-0.33	0.48	-551	-28
		<b>-0.39</b>	<b>0.16</b>		
E 500μm		0.46	0.50	646	-104
		0.43	0.47	646	-134
		<b>0.44</b>	<b>0.04</b>		
Southwest (±0.44; 2SD)	N 500μm	0.41	0.49	17	593
		0.27	0.51	17	623
		<b>0.34</b>	<b>0.20</b>		
S 500μm		-1.26	0.49	119	-855
		-1.09	0.50	119	-825
		<b>-1.17</b>	<b>0.23</b>		

*Continued on next page*

Table A2. Continued

		0.39	0.34	50	495
	N 500 $\mu$ m	0.49	0.37	80	495
		<b>0.44</b>	<b>0.13</b>		
		1.71	0.39	263	974
	N 1000 $\mu$ m	0.72	0.36	233	974
		<b>1.22</b>	<b>1.40</b>		
East					
( $\pm 0.28$ ; 2SD)					
	S 500 $\mu$ m	0.05	0.34	0	-500
		-0.48	0.36	-30	-500
		<b>-0.21</b>	<b>0.75</b>		
		-0.79	0.38	-243	-807
	S 800 $\mu$ m	-1.06	0.34	-273	-807
		<b>-0.92</b>	<b>0.38</b>		
		-0.07	0.27	43	-498
	S 500 $\mu$ m	-0.10	0.30	55	-517
		<b>-0.09</b>	<b>0.05</b>		
		0.42	0.27	500	0
	E 500 $\mu$ m	0.62	0.34	521	-24
		<b>0.52</b>	<b>0.28</b>		
		0.25	0.32	-1	485
West	N 500 $\mu$ m	0.46	0.31	73	495
( $\pm 0.22$ ; 2SD)		<b>0.35</b>	<b>0.29</b>		
		-0.47	0.31	-520	11
	W 500 $\mu$ m	-0.56	0.33	-506	-51
		<b>-0.52</b>	<b>0.13</b>		
		-0.74	0.38	-826	26
	W 1000 $\mu$ m	-0.84	0.41	-813	-8
		<b>-0.79</b>	<b>0.15</b>		
		-0.72	0.36	-483	-299
	S 300 $\mu$ m	-0.75	0.34	-499	-321
		<b>-0.73</b>	<b>0.04</b>		
Southeast					
( $\pm 0.30$ ; 2SD)					
		0.30	0.36	17	230
	N 300 $\mu$ m	0.06	0.36	47	230
		<b>0.18</b>	<b>0.35</b>		
		0.00	0.28	-119	267
Northeast ( $\pm$	NW 200 $\mu$ m	-0.16	0.27	-119	237
<b>0.19</b> ; 2SD)		<b>-0.08</b>	<b>0.23</b>		

\*Bold-faced numbers are average values and external reproducibility (2SD).

Table A3. Measured  $\delta^{18}\text{O}$  values relative to the center of the grains in individual holes in the 3-hole disk-3\*

Disk-3	$\delta^{18}\text{O} \pm 2\text{SE}$ (‰)		$\Delta X$	$\Delta Y$	
			(μm)		
N 500μm	-0.05	0.35	0	500	
	0.06	0.34	-30	500	
	<b>0.00</b>	<b>0.16</b>			
N 1000μm	0.31	0.32	0	1000	
	0.20	0.34	30	1000	
	<b>0.25</b>	<b>0.15</b>			
S 500μm	-0.25	0.35	-30	-500	
	-0.29	0.35	-60	-500	
	<b>-0.27</b>	<b>0.05</b>			
S 1000μm	-0.60	0.33	0	-1000	
	-0.41	0.37	-30	-1000	
	<b>-0.50</b>	<b>0.26</b>			
North (±0.29; 2SD)	S 1500μm	-0.89	0.36	-30	-1500
		-0.86	0.34	-60	-1500
		<b>-0.88</b>	<b>0.05</b>		
S 1800μm		-1.81	0.34	0	-1800
		-1.63	0.33	-30	-1800
		<b>-1.72</b>	<b>0.25</b>		
W 500μm		0.34	0.33	-500	0
		0.12	0.35	-500	30
		<b>0.23</b>	<b>0.30</b>		
E 500μm		0.33	0.35	500	0
		0.46	0.35	500	-30
		<b>0.40</b>	<b>0.19</b>		
E 900μm		0.18	0.40	900	0
		-0.09	0.34	900	-30
		<b>0.04</b>	<b>0.37</b>		

*Continued on next page*

Table A3. Continued

		0.16	0.35	90	530
	N 500 $\mu$ m	0.21	0.36	120	530
		<b>0.18</b>	<b>0.07</b>		
		0.04	0.38	197	940
	N 1000 $\mu$ m	0.16	0.37	197	910
		<b>0.10</b>	<b>0.17</b>		
		-0.18	0.36	499	1
	E 500 $\mu$ m	-0.08	0.37	499	-59
		<b>-0.13</b>	<b>0.15</b>		
		-0.09	0.33	792	-53
	E 800 $\mu$ m	-0.28	0.37	792	-83
		<b>-0.19</b>	<b>0.28</b>		
		-0.19	0.38	0	-500
Southwest	S 500 $\mu$ m	-0.12	0.38	-30	-500
( $\pm 0.31$ ; 2SD)		<b>-0.15</b>	<b>0.10</b>		
		-0.28	0.37	60	-1000
	S 1000 $\mu$ m	-0.19	0.39	90	-1000
		<b>-0.24</b>	<b>0.12</b>		
		-0.51	0.41	-1000	30
	W 1000 $\mu$ m	-0.35	0.34	-1000	60
		<b>-0.43</b>	<b>0.23</b>		
		-0.38	0.35	-940	1000
	NW 1000 $\mu$ m	-0.51	0.37	-910	1000
		<b>-0.45</b>	<b>0.19</b>		
		-0.02	0.37	900	-900
	SE 900 $\mu$ m	-0.40	0.35	900	-870
		<b>-0.21</b>	<b>0.54</b>		

*Continued on next page*

Table A3. Continued

		-0.21	0.31	500	-30
	E 500 $\mu\text{m}$	-0.10	0.34	500	-60
		<b>-0.15</b>	<b>0.16</b>		
		-0.57	0.29	1000	-270
	E 1000 $\mu\text{m}$	-0.31	0.31	1000	-300
		<b>-0.44</b>	<b>0.36</b>		
		-0.47	0.33	1200	-430
	E 1200 $\mu\text{m}$	-0.47	0.33	1200	-405
		<b>-0.47</b>	<b>0.01</b>		
		-0.01	0.28	-700	0
	W 700 $\mu\text{m}$	-0.16	0.31	-700	-30
		<b>-0.09</b>	<b>0.21</b>		
		-0.07	0.32	-1000	0
	W 1000 $\mu\text{m}$	-0.19	0.35	-1000	-30
		<b>-0.13</b>	<b>0.17</b>		
		-0.08	0.33	-1300	0
Southeast	W 1300 $\mu\text{m}$	-0.03	0.31	-1300	30
( $\pm 0.25$ ; 2SD)		<b>-0.06</b>	<b>0.08</b>		
		0.05	0.32	-1330	900
	NW 1300 $\mu\text{m}$	-0.13	0.33	-1330	870
		<b>-0.04</b>	<b>0.25</b>		
		0.08	0.35	0	1000
	N 1000 $\mu\text{m}$	-0.25	0.32	-30	1000
		<b>-0.09</b>	<b>0.47</b>		
		0.27	0.32	270	1200
	NE 1200 $\mu\text{m}$	-0.12	0.35	300	1200
		<b>0.08</b>	<b>0.55</b>		
		-0.92	0.32	-530	-1130
	SW 1200 $\mu\text{m}$	-0.81	0.30	-560	-1160
		<b>-0.86</b>	<b>0.16</b>		
		-1.12	0.34	-757	-1502
	SW 1600 $\mu\text{m}$	-1.10	0.36	-787	-1502
		<b>-1.11</b>	<b>0.02</b>		

\*Bold-faced numbers are average values and external reproducibility (2SD).

Table A4. Measured  $\delta^{18}\text{O}$  values relative to the center of the grains in individual holes in the 3-hole disk-4\*

		-0.23	0.22	-1000	0
	W 1000 $\mu\text{m}$	0.05	0.23	-1000	30
		<b>-0.09</b>	<b>0.40</b>		
		0.04	0.27	1000	0
	E 1000 $\mu\text{m}$	-0.04	0.24	970	0
		<b>0.00</b>	<b>0.11</b>		
North					
( $\pm 0.16$ ; 2SD)					
	N 1000 $\mu\text{m}$	0.14	0.24	0	1000
		0.18	0.25	-30	1000
		<b>0.16</b>	<b>0.06</b>		
		-0.48	0.24	0	-1000
	S 1000 $\mu\text{m}$	-0.25	0.21	30	-1000
		<b>-0.36</b>	<b>0.32</b>		
		0.43	0.44	12	913
	N 1000 $\mu\text{m}$	0.43	0.43	38	904
		<b>0.43</b>	<b>0.00</b>		
		0.09	0.42	-967	66
	W 1000 $\mu\text{m}$	-0.18	0.41	-966	41
		<b>-0.05</b>	<b>0.39</b>		
Southwest					
( $\pm 0.37$ ; 2SD)					
	E 300 $\mu\text{m}$	0.33	0.40	290	36
		-0.12	0.46	279	10
		<b>0.10</b>	<b>0.63</b>		
		-0.41	0.40	-42	-363
	S 400 $\mu\text{m}$	-0.22	0.41	-48	-384
		<b>-0.32</b>	<b>0.26</b>		
		-0.57	0.37	-1000	0
	W 1000 $\mu\text{m}$	-0.66	0.34	-1000	-30
		<b>-0.62</b>	<b>0.13</b>		
		-0.04	0.36	0	700
Southeast	N 700 $\mu\text{m}$	0.09	0.35	-30	700
( $\pm 0.26$ ; 2SD)		<b>0.02</b>	<b>0.18</b>		
		0.64	0.36	-700	700
	SW 700 $\mu\text{m}$	-0.21	0.39	-730	700
		<b>0.22</b>	<b>1.20</b>		

\*Bold-faced numbers are average values and external reproducibility (2SD).

Table A5. Oxygen isotope ratios of the chondrule Ch09 from SaU 290 measured with 4  $\mu\text{m}$  spots, using the 7-hole disks (disk-1) and IMS-1280 SIMS\*

	$\delta^{18}\text{O} \pm 2\text{SE} (\text{‰})$		$\delta^{17}\text{O} \pm 2\text{SE} (\text{‰})$		$\Delta^{17}\text{O} \pm 2\text{SE} (\text{‰})$		$^{16}\text{O}$ ( $10^6$ cps)
SC-O1	2.36	0.50	3.03	1.22	1.80	1.25	18.9
	1.24	0.67	2.58	1.14	1.94	1.19	18.4
	1.28	0.60	1.78	1.12	1.12	1.16	18.2
Ch09	-2.19	0.93	-6.37	1.80	-5.24	1.86	9.0
	-3.56	0.78	-9.17	1.80	-7.32	1.84	10.7
	-8.86	0.88	-10.21	1.24	-5.60	1.32	11.1
	-11.47	0.77	-13.33	1.83	-7.37	1.88	11.0
SC-O1	2.11	0.46	3.69	0.94	2.59	0.97	18.4
	1.99	0.52	2.81	1.11	1.78	1.14	17.9
	1.23	0.58	3.65	1.31	3.02	1.34	17.7
	<b>1.70</b>	<b>1.02</b>	<b>2.92</b>	<b>1.43</b>	<b>2.04</b>	<b>1.34</b>	<b>18.3</b>

\*Oxygen isotope ratios of Ch09 are corrected for instrumental bias. Bold-faced numbers are average values of bracketing standard analyses and external reproducibility (2SD).